Eclética Química Journal

Original article
iq.unesp.br/ecletica

| Vol. 44 | n. 4 | 2019 |

Influence of Ce(IV) ions amount on the electrochemical behavior of organic-inorganic hybrid coatings in 0.1 mol L^{-1} NaCl solution

Fernando Santos da Silva[1], Hercílio Gomes de Melo[2], Assis Vicente Benedetti[1], Patrícia Hatsue Suegama[3+]

[1] São Paulo State University (Unesp), Institute of Chemistry, 55 Prof. Francisco Degni St, Araraquara, São Paulo, Brazil
[2] University of São Paulo (USP), 2463 Professor Mello Moraes Av, Butantã, São Paulo, São Paulo, Brazil
[3] Faculty of Exact Sciences and Technology (UFGD), Dourados Hw - Itahum, km 12, Mato Grosso, Brazil

[+]Corresponding author: Patrícia Hatsue Suegama, email address: patriciasuegama@ufgd.edu.br

ARTICLE INFO

Article history:
Received: January 9, 2019
Accepted: May 14, 2019
Published: October 1, 2019

Keywords:
1. cerium
2. corrosion
3. organic-inorganic hybrid coating
4. EIS

ABSTRACT: In this work, the influence of ceric ions ($Ce(SO_4)_2$) addition to the hydrolysis solution on the corrosion protection afforded by organic-inorganic hybrid coating obtained from tetraethoxysilane (TEOS) and 3-methacryloxy-propyl-trimethoxysilane (MPTS) to a carbon steel substrate in 0.1 mol L^{-1} NaCl solution was studied. Open circuit potential (E_{OC}) and electrochemical impedance spectroscopy (EIS) experiments were carried out and showed that the protection afforded by the organic-inorganic hybrid coating was extremely dependent on the Ce^{4+} ions amount. These results were in close agreement with optical microscopy observation of the degrading surfaces, both procedures showing that more protective coating was produced when 500 ppm of Ce^{4+} ions were added to the organic-inorganic hybrid solution. The chemical state of the organic-inorganic hybrid coating investigated by X-ray photoelectron spectroscopy (XPS) indicated that the addition of Ce^{4+} ions enhances the polycondensation degree of the organic-inorganic hybrid coating leading to a denser siloxane (Si-O-Si) network. A strategy using laser-induced breakdown spectroscopy (LIBS) and UV-Vis spectrometry was set up in order to verify, respectively, the presence of Ce ions within the coating structure and its oxidation state. LIBS results confirmed the incorporation of Ce ions in the coating, which, according to UV-Vis measurements, are mainly in the (IV)-oxidation state.

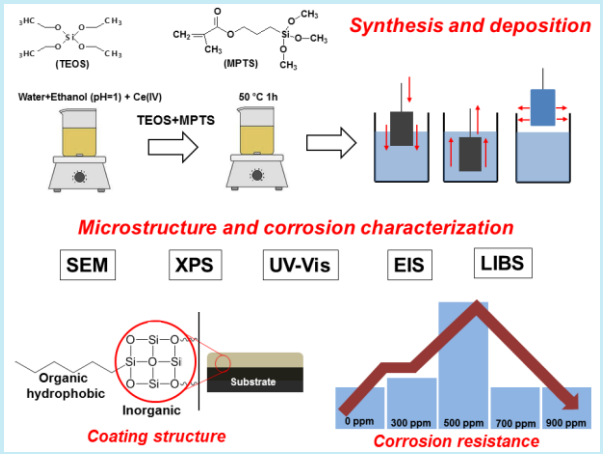

1. Introduction

Organic-inorganic hybrid coating has been investigated as a new alternative for substitution of chromium-based coatings and paints for corrosion protection of several metallic substrates[1-10]. The organic-inorganic hybrid coatings are environmentally friendly, have low cost, good adhesion, high corrosion resistance and are easily and rapidly prepared.

Organic-inorganic hybrid coating can be obtained by sol-gel process in two steps: initially, in the hydrolysis step, hydrolysable groups of the precursors are converted to silanol groups (Si-OH)[2]. In the second step condensation reactions of silanol groups between themselves or with hydroxyl rich metallic surface lead to formation, respectively, of siloxane (Si-O-Si) and metalo-siloxane (Me-O-Si) bonds. Thus, a highly adherent and cross-linked structure is obtained forming a physical barrier on the metal surface, which

ISSN: 1678-4618
DOI: 10.26850/1678-4618eqj.v44.4.2019.p27-56

prevent electrolyte from reaching the substrate. However, the efficiency of this barrier protection effect is limited due to formation of small pores, microcracks, and water uptake of the coating[4-7]. In order to improve the protection provided by these coatings the modification of the organic-inorganic precursor solution using corrosion inhibitors like nanoparticles and cerium ions has been proposed[1,2,6-10].

The use of ceric sulfate, in the modification of polymers and organic-inorganic hybrid materials by redox polymerization reaction is a widely used method with industrial importance[11-16]. For organic-inorganic hybrid materials, it is proposed that silanol molecules (R1-Si-$(OH)_3$) and alcohol from the hydrolyzed precursors can complex with Ce^{4+} ions to produce free radicals, thus increasing the polymerization and the polycondensation degree of the siloxane (Si-O-Si) network[17-22].

The effect of cerium ions in the performance of organic-inorganic hybrid coatings was previously described[8-10,12,19-22]. Ferreira *et al.*[8] have used rare earth (Ce, La) salts and bis-sulfur silane (BTESPT) as chromate substitutes for galvanized steel, resulting in improvement of corrosion resistance and paint adherence. The effect of cerium in the corrosion protection of galvanized steel by doping with cerium (III) nitrate silane solutions was discussed based in the self-healing effect due to the cerium oxide precipitation[9]. Montemor *et al.*[10] investigated the electrochemical behavior of galvanized steel substrates pre-treated with bis-[triethoxysilylpropyl]tetrasulfide silane (BTESPT) solutions modified with SiO_2 or CeO_2 nanoparticles. The presence of nanoparticles reinforced the barrier properties of the silane coating and suggested a synergism between the activated nanoparticles and cerium ions, that reduced the corrosion activity. Suegama *et al.*[19] have evaluated the effect of low amount of Ce^{4+} ions (≈ 50 ppm) addition on the polymerization of bis-[triethoxysilyl]ethane (BTSE) coating applied on carbon steel. The coating characterization showed a better surface finishing and a higher thickness for the coatings doped with Ce^{4+} ions enhancing the barrier properties provided by the coating alone. Palomino *et al.*[20] have studied the performance of bis-1, 2-(triethoxysilyl) ethane (BTSE) doped with a mixture of Ce^{4+} ions and silica nanoparticles as a pre-treatment to protect the AA 2024-T3 against corrosion. The addition of Ce^{4+} ions increased the degree of surface coverage and improved the anticorrosion properties of the doped coating. Hammer *et al.*[21] have investigated hybrid coatings prepared by tetraethoxysilane (TEOS), 3-methacryloxy propyltrimethoxysilane (MPTS), doped with Ce^{3+} and Ce^{4+} ions deposited onto 316L stainless steel. The XPS results indicate an increase in the network connectivity related to the active role of Ce^{4+} ions in the polymerization of siloxane groups and the improvement of the corrosion resistance of Ce^{4+} doped organic-inorganic hybrid coating. The effect of the addition of Ce^{4+} ions was also performed using structural analyzes of Si RMN[22]. The results showed that the T3 ($Si(OSi)_3R'$) and Q4 ($Si(OSi)_4$) resonance bands were more intense in the hybrids modified with Ce^{4+} ions, indicating a structure with a denser Si-O-Si network, thus producing more resistive, thicker and less porous materials. According to the literature[12,19-22], the improved protection characteristics of the hybrid is attributed to the effect of Ce^{4+} ions in the polymerization rate of the organic phase and in the polycondensation of the siloxane structure, producing more condensed and crosslinked polymeric networks. Authors also reported that hydroxyl groups from alcohol molecules can form complexes with Ce^{4+} ions, which decomposes to form free radicals, contributing to the hybrid polymerization[22].

This work aims at studying the influence of different amounts of Ce^{4+} ions added to tetraethoxysilane (TEOS) and 3-methacryloxy-propyl-trimethoxysilane (MPTS) organic-inorganic hybrid coating deposited on carbon steel and evaluating its corrosion resistance during relative long immersion times in NaCl 0.1 mol L^{-1} using electrochemical impedance spectroscopy (EIS) and open circuit potential (E_{OC}) measurements. As far as authors are aware, there is no work carried out to identify the presence of Ce ions inside the organic-inorganic hybrid coating using Laser-induced breakdown spectroscopy (LIBS) as well the use of UV-Vis analysis to investigate the Ce oxidation state inside this coating.

2. Materials and methods

2.1. Metallic substrate and solutions

The metallic substrate used was a SAE 1020 carbon steel (20 × 22 × 1.2 mm) with the composition C (0.40 wt.%), Mn (0.30 wt.%), Si (0.03 wt.%) and Fe balance, determined using an EDX-720/800HS Energy Dispersive X-ray

Eclética Química Journal, vol. 44, n. 4, 2019, 27-56
ISSN: 1678-4618
DOI: 10.26850/1678-4618eqj.v44.4.2019.p27-56

Fluorescence Spectrometer, SHIMADZU. Initially the samples were ground with 320, 600 and 1200 grit silicon carbide emery paper, washed with distilled water and dried in purified air. Afterwards, they were sonicated in ethyl alcohol for 10 min and dried in hot air stream.

2.2. Coating preparation and coating thickness

The synthesis of the TEOS and MPTS organic-inorganic hybrid coating modified with 0, 300, 500, 700 or 900 ppm Ce^{4+} ions was performed via the sol-gel process in two steps. Initially, 6.8 mL of an ethanol/water solution (62/38% v / v) at pH 1.0 was used to solubilize the desired amount of cerium salt ($Ce(SO_4)_2$) under stirring, until a colorless solution was obtained. In the second step 6 mL of TEOS (Sigma Aldrich 99.8%) and 3.2 mL of MPTS (Fluka 99.8%) were added together to the solution prepared in the first step, and the mixture was stirred for 1 h at 50 °C. The solution of the organic-inorganic hybrid just before deposition on steel had a final pH 4. All coatings were applied by dip coating at a constant immersion / withdrawal rate of 14 cm min^{-1} with three dips, with intervals of 1 min between each one of them. The curing step consisted in heating at 50 °C for 24 h followed by 3 h at 160 °C. The coating thickness was measured by optical interference using a FILMETRICS F3-CS with 2 nm resolution. The thicknesses of TEOS/MPTS organic-inorganic hybrid coatings were measured at three different regions, and the average values were: 728±2 nm (0 ppm); 748±3 nm (300 ppm); 843±8 nm (500 ppm); 736±8 nm (700 ppm) and 789±5 nm (900 ppm).

2.3. Electrochemical measurements

The protection of the substrate provided by the coatings was investigated in 0.1 mol L^{-1} NaCl solution using EIS and E_{OC} measurements. The measurements were performed during 120 h for the substrate and for different times for coatings containing the following cerium additions / ppm: 0 (144 h); 300 (192 h); 500 (688 h); 700 (144 h) and 900 (172 h). For these coatings, the testing time corresponds to an abrupt change of E_{OC} values, suggesting that the electrolyte has reached the substrate. EIS measurements were done in the frequency range from 100 kHz to 10 mHz, by applying a sinusoidal potential perturbation of 10 mV (rms) *vs*. E_{OC}, and were performed after 1 h, 8 h and every 24 h of immersion until visual failure of the samples. Therefore, EIS measurements were conducted until the resistance of the coating was very low, and no more protection of the substrate was afforded. Equivalent Electric Circuit (EEC) fitting using the Z-view® software was employed for quantitative analysis of the EIS responses. Before the fitting procedure, the consistency of the experimental data was verified using the Kramers-Kronig Transform (KKT)[23]. The fittings were carried out only for the experimental points in the frequency region where there was concordance with the KKT treatment.

2.4. Surface characterization and analytical techniques

2.4.1 SEM-EDS and AFM analysis

Morphological characterization using optical micrograph images was performed for all samples during the electrochemical measurements. Images of scanning electron microscopy and EDS analysis were obtained using a JEOL JSM-5310 coupled with energy dispersive X-ray spectroscopy analysis (SEM / EDS). The micrographs were acquired prior to and after 240 h immersion in the chloride medium for the sample protected with the nondoped organic-inorganic hybrid coating and after ≈ 400 h for the organic-inorganic hybrid coating with the Ce^{4+} quantity that showed the best anticorrosion protection. The accelerating voltage used to perform the EDS analysis was 15 keV.

The morphologies of TEOS / MPTS coatings prepared with 300 ppm of Ce^{4+} or Ce^{3+} ions were also analyzed by Atomic Force Microscopy (AFM) to compare the effects of the Ce ions oxidation state on the coating morphology. An AFM model Agilent 5500 was used to acquire the images in the intermittent mode and using a pyramidal tip. All images were done in 5 μm^2 area.

2.4.2 X-Ray Photoelectron spectroscopy (XPS) analysis

Structural characterization of the coatings was performed using a UNI-SPECS UHV instrument for organic-inorganic hybrid-coated samples without Ce and with the doped condition with the best anticorrosion performance. The samples were fixed on small flat discs on a XYZ manipulator and placed in the analysis chamber, which residual pressure was maintained below 10^{-8} Torr while data were being obtained. The Mg Kα line was used

Eclética Química Journal, vol. 44, n. 4, 2019, 27-56
ISSN: 1678-4618
DOI: 10.26850/1678-4618eqj.v44.4.2019.p27-56

(hν = 1253.6 eV) and the analyzer pass energy was set to 10 eV. XPS was used to investigate the core level of C 1s, O 1s, Si 2p. The intensities were estimated by calculating the area under each peak after smoothing and subtraction of the shaped background and fitting the experimental curve to a combination of Lorentzian and Gaussian lines of variable proportions.

2.4.3 Laser-induced breakdown spectroscopy (LIBS) analysis

LIBS was also used to analyze the organic-inorganic hybrid coatings without Ce^{4+} ions and doped with 1500 ppm of Ce^{4+} ions prepared in the same conditions of the other organic-inorganic hybrid coatings (*subsection 2.2*) and deposited onto copper substrate. This strategy was adopted, since iron from the substrate exhibits strong interference in the Ce analysis[24]. The spectra of the samples were acquired with a LIBS 2500plus spectrometer (Ocean Optics, Dunedin, FL, USA), which uses a Q-switched Nd:YAG laser at 1064 nm (Quantel, Bozeman, MT, USA) operating at 75 mJ maximum power energy, 8 ns pulse width, and 10 Hz frame rate. The laser pulse was focused on the sample inside an ablation chamber. After the plasma was formed, the emission of excited species was carried out by an optical fiber bundle connected to seven spectrometers ranging from 188 to 980 nm, each one coupled with a 2048 nm element linear silicon CCD array, whose resolution was ~0.1 nm (FWHM). The distance from the sample to the collecting optical fiber bundle was approximately 7 mm. All measurements were performed in air, and the LIBS system was set to 50 mJ per laser pulse with a 2.1 ms integration time and a fixed delay time of 2 μs. 10 measurements were carried out on each sample.

2.4.4 UV-Vis measurements

To perform the UV-Vis measurements freestanding cerium nitrate ($Ce(NO_3)_3$) and ceric sulfate ($Ce(SO_4)_2$) doped organic-inorganic hybrid coatings (300, 500 and 900 ppm) were prepared by pouring the hydrolysis solution into a crucible and then curing as previously described (*subsection 2.2*). Afterwards, 3 g of each coating were ground and placed in test tubes with 3 mL of distilled water for 15 days. Then, the extract was filtered (pore size < 25 μm) and the solution analyzed in the UV-Vis region. Water was used as reference and spectra were also obtained from solutions of 200 ppm of $Ce(SO_4)_2$ or $Ce(NO_3)_3$ in distilled water. Two solutions were also prepared by extracting Ce, in argon atmosphere, from the coating doped with Ce^{4+} or Ce^{3+} ions, and immediately analyzed. UV-Vis measurements of freestanding solid organic-inorganic hybrid coating were also carried out. Organic-inorganic hybrid coating with 0 and 500 ppm of Ce^{4+} ions were deposited onto glasses. For comparison UV-Vis measurements of the glass and crystals of $Ce(SO_4)_2$ were also performed. The spectra were obtained with an UV/VIS Lambda 265 (Perkin Elmer) or an UV/Vis/NIR (Perkin Elmer) spectrophotometer from 190 to 1100 nm with spectral resolution of 2 nm and using a polished four-face quartz cuvette with a light path length of 10 mm for measuring in solution. Special care was taken to obtain the spectra considering the complexity of the UV-Vis response of Ce^{4+} and Ce^{3+} ions systems that show, respectively, charge transfer and f-d transitions, which are strongly influenced by the environment. Therefore, only spectra obtained at the same conditions were compared.

3. Results and discussion

3.1. Electrochemical measurements

E_{OC} evolution after different immersion times for the uncoated and coated substrates are presented in Fig. 1. All samples protected with the organic-inorganic hybrid coating showed E_{OC} more positive than the bare substrate, indicating that the electrochemical response was modified. The sample doped with 500 ppm of Ce^{4+} ions provided the noblest potential (0.4±0.1) V/(Ag/AgCl/KCl_{sat}) at initial immersion times, suggesting the formation of a denser cross linked coating, and the best protective character[13,16,21]. This E_{OC} value also indicates that the barrier effect of the coating doped with 500 ppm of Ce^{4+} ions induced a higher ohmic drop compared to the bare substrate and other coatings. After 432 h, the E_{OC} abruptly decreases to -0.6 V/(Ag/AgCl/KCl_{sat}), very close to that E_{OC} of the substrate, suggesting that the electrolyte may have reached the coating/substrate interface. Other coatings showed at initial immersion times E_{OC} values close to -0.4 V/(Ag/AgCl/KCl_{sat}), and at times less than 200 h the E_{OC} values were almost the same of the substrate, indicating electrolyte uptake by the coating and coating degradation as verified by other studies[25].

Eclética Química Journal, vol. 44, n. 4, 2019, 27-56
ISSN: 1678-4618
DOI: 10.26850/1678-4618eqj.v44.4.2019.p27-56

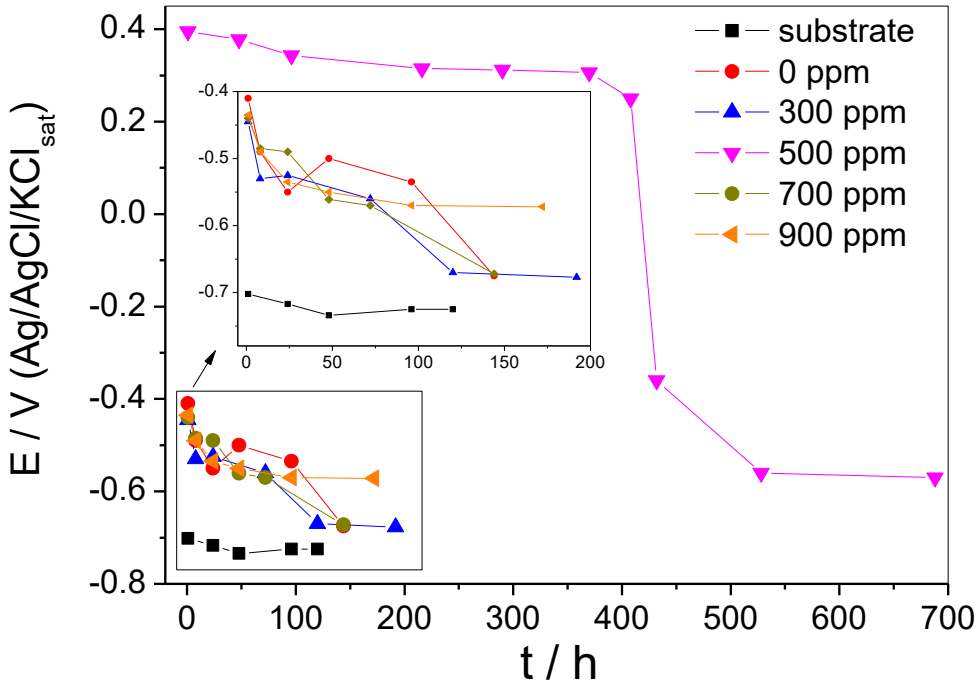

Figure 1. E_{OC} variation in 0.1 mol L^{-1} NaCl solution for bare carbon steel and for samples protected with TEOS / MPTS organic-inorganic hybrid coatings modified with different amounts of Ce^{4+} ions.

Fig. 2 shows the Bode plots for all studied samples. The phase angle diagrams for the bare substrate showed basically one time constant centered at around 5 Hz (Fig. 2A) due to iron oxidation. For the sample protected with the nondoped coating, two time constants can be clearly identified (Fig. 2B). The high frequency (HF) one is related to the organic-inorganic hybrid coating, and the other, in the low frequency (LF) domain, is attributed to the interfacial response (double layer charging in parallel with the charge transfer resistance)[16,22,26]. For the coatings doped with Ce^{4+} ions (Fig. 2C-2F) a third-time constant appeared in the medium frequency (MF) range. This feature was associated to the presence of Ce species within the organic-inorganic hybrid coating, presenting a different relaxation behavior than that exhibited by the coating and the substrate. In the HF region, phase angles close to -90° were always obtained for short immersion times, indicating good barrier properties of the coating. Afterwards a slow decay was observed for longer immersion periods that can be related to coating degradation due to electrolyte uptake[27]. The decaying rate is directly proportional to the coating protection capability: the more protective the coating the slower the HF phase angle reduction. Concomitantly, a reduction of the LF impedance modulus occurs at variable rate depending on the sample, indicating the progress of corrosion processes at the interface.

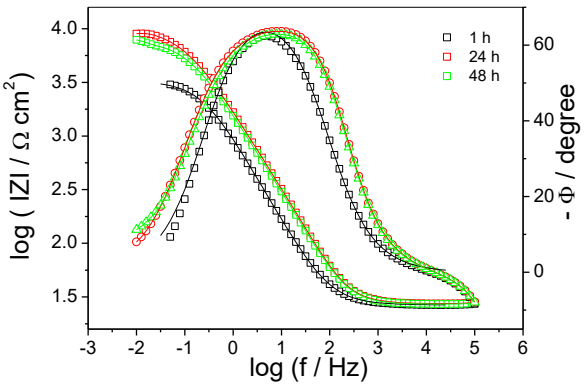

2A

Eclética Química Journal, vol. 44, n. 4, 2019, 27-56
ISSN: 1678-4618
DOI: 10.26850/1678-4618eqj.v44.4.2019.p27-56

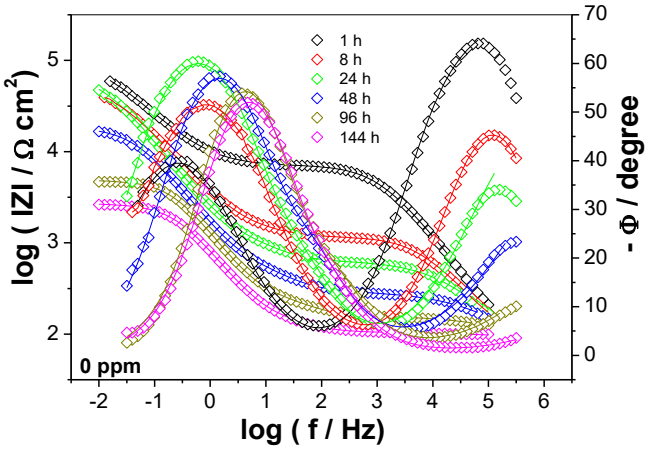

2B

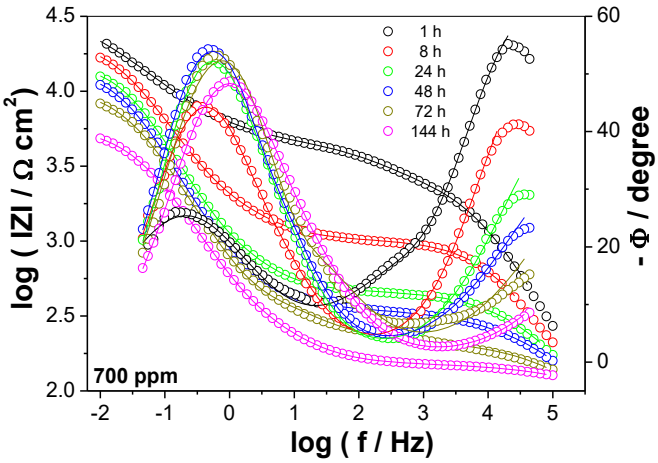

2E

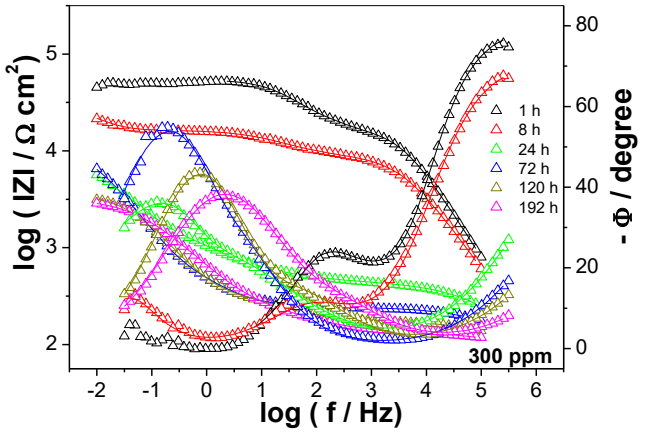

2C

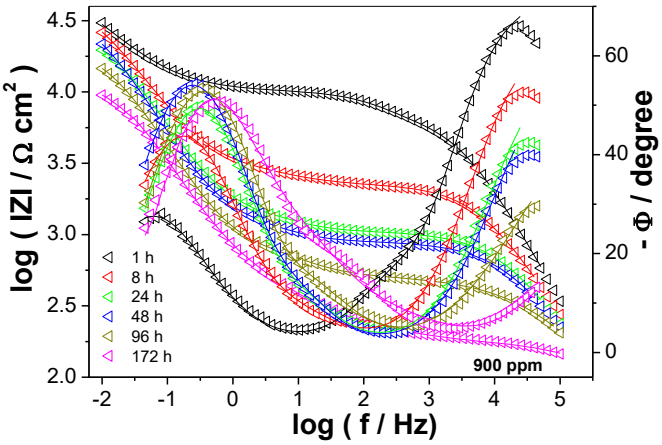

2F

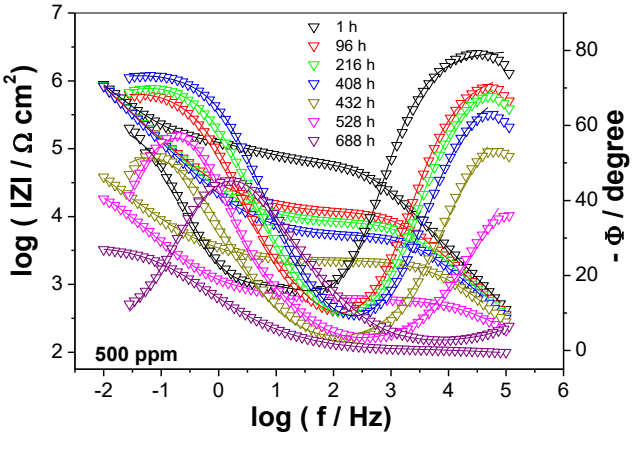

2D

Figure 2. Experimental (symbols) and fitted (solid line) Bode plots for (**A**) bare carbon steel, and for carbon steel coated with TEOS / MPTS organic-inorganic hybrid coating doped with different Ce^{4+} ions concentration / ppm: (**B**) 0, (**C**) 300, (**D**) 500, (**E**) 700 and (**F**) 900, for different immersion times in 0.1 mol L^{-1} NaCl.

The addition of Ce^{4+} ions seems to play a conflicting role in the anticorrosion properties of the organic-inorganic hybrid coatings (Fig. 2 and Fig. 1S, Supplementary data). For some formulations (500 and 900 ppm) the doped coating presented higher impedance than the nondoped one, whereas for others (300 and 700 ppm) the doping procedure damaged the protective properties of the coating.

In previous works[10,21,22,28], it has been reported that the addition of Ce^{4+} ions to the hydrolysis solution provides an increase of the silanol groups condensation rate to form a denser and cross-linked

Eclética Química Journal, vol. 44, n. 4, 2019, 27-56
ISSN: 1678-4618
DOI: 10.26850/1678-4618eqj.v44.4.2019.p27-56

coating. In addition, in organic chemistry, these ions are often used for the oxidation of alcohols [15-18,29,30]. The proposed general mechanism for such reaction shows that Ce^{4+} ions form complexes with the ethanol molecules, which, when decomposed, form free radicals that react with each other leading to the polymerization of ethanol and / or silanol by a polymerization redox reaction[16,19]. This redox polymerization process is characteristic of ethanol in the presence of Ce^{4+} ions. The complexes may react with each other via free radical reactions leading to polymerization, in a similar way as the generic mechanism previously presented[16]. The effect of Ce^{4+} ions in the coating formation would be twofold, besides increasing the polymerization rate it would also promote the formation of silanol groups as it shifts to the right the equilibrium of the hydrolysis reaction (silanol formation). Therefore, the effect of Ce^{4+} ions is to increase the reaction rate among silanol groups leading to the formation of more densely cross linked coating[19,29-31]. The redox polymerization of Ce^{4+} ions also leads to the formation of Ce^{3+} ions[19,29-31]. However, the amount of this latter ion being formed is insignificant, and it would not be reasonable to consider an inhibiting contribution effect due to the presence of Ce^{3+} ions in the organic-inorganic hybrid solution/coating in accordance with other authors[2,22,28]. In addition, the molecule of MPTS can react with Ce^{4+} ions by redox polymerization due to the radical polymerization process (see Supplementary data). The MPTS molecule reacts with Ce^{4+} ions forming the radical species of MPTS and reducing Ce^{4+} to Ce^{3+} ions (Fig. 1S, Supplementary data). After that occurs successive additions of monomer to radical, and the termination stage occurs with mutual reactions of two radicals to form an inactive polymer and can occur by combination. It has been reported that the thickness of the organic-inorganic hybrid coating increases in the presence of cerium ions, which may result in higher impedance values for modified coating[10,19-21]. Therefore, it would be expected a steady increase of the impedance modulus for increasing Ce^{4+} ions amounts added to the hydrolysis solution.

However, this was not verified in the present work where a thicker coating was obtained for the hydrolysis solution modified with 500 ppm of Ce^{4+} ions, which also presented the best anticorrosion behavior. It happens likely because the addition of Ce^{4+} ions to the hydrolysis solution above a certain amount may lead to the decrease in the rate of redox polymerization and crosslink formation[21,29]. This results from the inactivation of the active initiator species due to excess Ce^{4+} ions concentration bringing about premature termination[21,29].

As evidenced in Fig. 2B and 2C the addition of 300 ppm of Ce^{4+} ions to the hydrolysis solution produced an organic-inorganic hybrid coating with lower protection capabilities than the blank coating (organic-inorganic hybrid coating without Ce^{4+} ions). In addition, a complex impedance response was verified, particularly for short immersion periods, where an inductive loop was observed in the LF domain (Fig. 1SA and 1SB, Supplementary data). The literature shows that an inductive LF response is obtained when iron dissolves in acidic electrolyte[32-35]. This has been ascribed to a dissolution path involving the formation of adsorbed species[33,34]. When dipping the substrate in the hydrolysis solution, bonding of the silanol functionality to the carbon steel surface must compete with its dissolution by the acidic electrolyte. Hence, if the adsorption process is not very fast, acidic attack of the metal surface can take place during the coating deposition and remnants of the acidic hydrolysis solution may remain entrapped beneath the coating. This could lead to the attack of the substrate by the residual acid during the initial stages of immersion in the NaCl solution, as suggested by the shape of the Nyquist diagram after 1 h immersion (Fig. 1S, Supplementary data).

When larger amounts of Ce^{4+} ions (700 and 900 ppm) were used, a lesser protection of the substrate was also observed, as lower values of $|Z|_{(f = 10\ mHz)}$ were obtained after 1 h of immersion (about 25 and 32 kΩ cm^2 – Fig. 2E and 2F) when compared to the coating modified with 500 ppm (Fig. 2D, $|Z|_{(f = 10\ mHz)}$ = 100 kΩ cm^2). These results are in accordance with the thicknesses determination that showed that the thickest layer was obtained when 500 ppm of Ce^{4+} ions was added to the hydrolysis solution. For higher concentrations (700 and 900 ppm) it is considered that a lower degree of polycondensation degree of the siloxane bonds might occur due to the large proportion of Ce^{4+} ions added to the hydrolysis solution[16,22,29,36]. This means that the increase of cerium (IV) amount may provide more chances for premature termination of the growing chain radicals, and hence the polymerization degree is decreased[14-16]. The hydroxyalkyl free radicals, which are extremely reactive towards cerium (IV) species, can have an oxidative termination of their

Eclética Química Journal, vol. 44, n. 4, 2019, 27-56
ISSN: 1678-4618
DOI: 10.26850/1678-4618eqj.v44.4.2019.p27-56

primary free radicals generated in the initiation step[16].

The impedance data were fitted using EECs to have a better understanding about the protective behavior of the coatings and their degradation. In the EIS diagrams of Fig. 2, symbols and lines correspond, respectively, to the experimental and fitted diagrams. EECs combine the use of elements such as resistors, constant phase elements, capacitors, inductors, and others. To be meaningful each passive element must have a physical-chemical association with an interfacial process. In addition, the fitting procedure must provide low chi-squared (χ^2) and low errors for each estimated value of the passive elements[27,37]. The EEC of Fig. 3A, composed of two time constants, was used to fit the EIS data of the sample coated with nondoped TEOS / MPTS. The values for each fitted parameter for different immersion times are presented in Table 1S (Supplementary data). The good fit to the experimental results (Fig. 3B) suggests that it may physically represent the behavior of this sample.

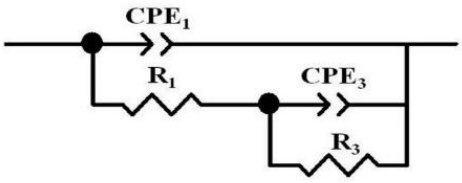

(Figure 3A)

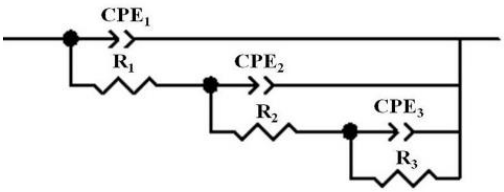

(Figure 3B)

Figure 3. Electrical equivalent circuits used to fit the impedance data for carbon steel coated with TEOS / MPTS with no doping (**A**) and doped with Ce^{4+} ions (**B**).

For the HF time constant, attributed to the organic-inorganic hybrid coating, CPE_1 is a constant phase element associated with the coating admittance (CPE_1-T) and a value of $\alpha_1 \neq 1$ (CPE_1-P) can be related to a nonuniform permittivity across the coating thickness due to electrolyte uptake[33,38-40]. The subcircuit associated with the organic-inorganic hybrid coating is completed with R_1 that represents the pore resistance. In the LF region, the time constant represented by the subcircuit CPE_3 in parallel with R_3, is related to the double layer admittance and the charge transfer resistance. In this case, a value of $\alpha_3 \neq 1$ suggests a heterogeneous charge distribution at the surface due to surface roughness, adsorption of species or defects on the sample surface[40-42].

For the nondoped coating a gradual increase in the value of CPE_1-T (related to the coating capacitance) is observed for increasing immersion times (Table 1S, Supplementary data), indicating progressive electrolyte uptake by the coating[41,42]. Concomitantly the pore resistance R_1 decreases (Fig. 4A) indicating the enlargement / multiplication of conductivity pathways through the coating.

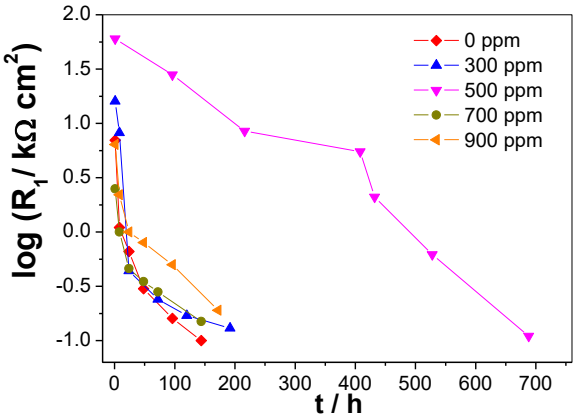

(Figure 4A)

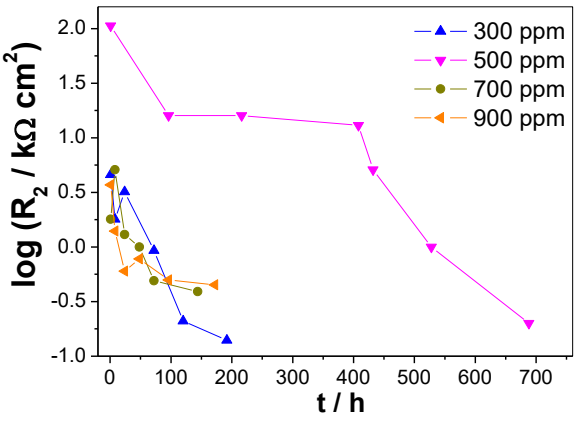

(Figure 4B)

Eclética Química Journal, vol. 44, n. 4, 2019, 27-56
ISSN: 1678-4618
DOI: 10.26850/1678-4618eqj.v44.4.2019.p27-56

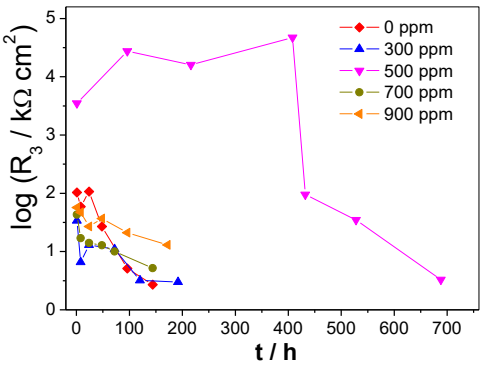

(**Figure 4C**)

Figure 4. Resistance values for the different time constants of the electrical equivalent circuits presented in Fig. 3 for doped and nondoped coating: (**A**) R_1, pore resistance; (**B**) R_2, resistance of the cerium oxide/ions within the organic-inorganic hybrid coating and (**C**) R_3, charge transfer resistance.

Accordingly, pit formation can be observed after 24 h, which must be a consequence of coating disruption (Fig. 5A). This can be assisted by the hydrolysis of the siloxane bonds within the coating, further increasing its degradation. Sakai *et al.*[41] also attributed the decrease of the pore resistance with immersion time to the shift of the chemical equilibrium of the hydrolysis reactions occurring with water. From 48 h a great decrease of R_3 was verified (Fig. 5C), indicating enhanced corrosion activity at the interface, which was confirmed by the photos taken of the electrode surface showing large amount of corrosion products (Fig. 5A).

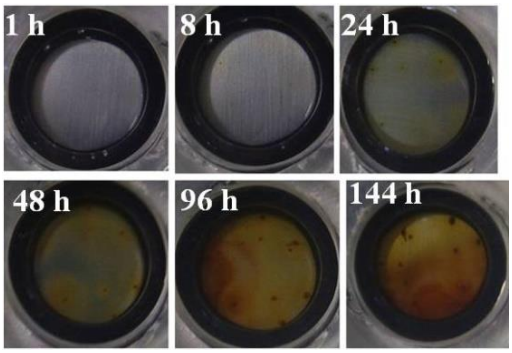

(Figure 5A)

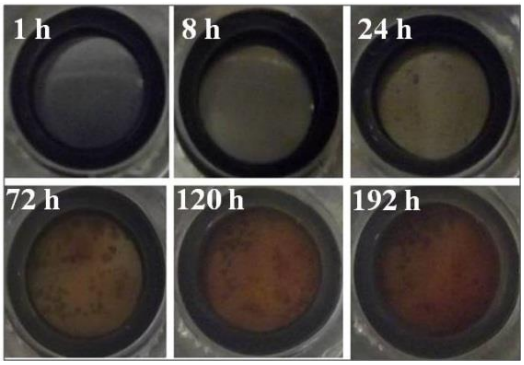

(Figure 5B)

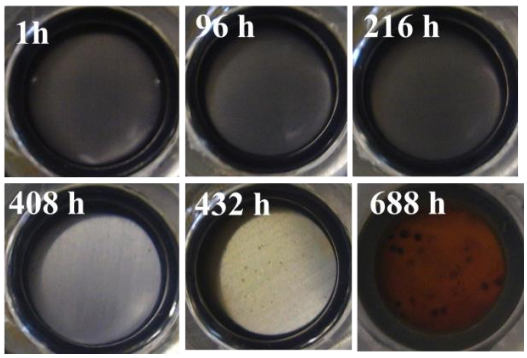

(Figure 5C)

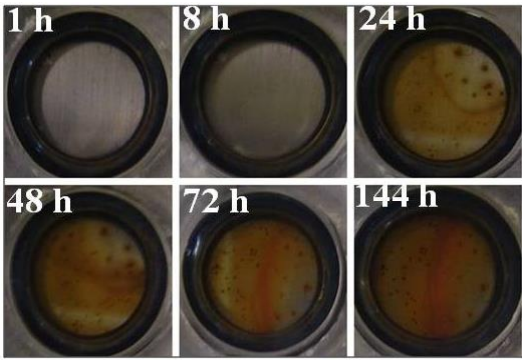

(Figure 5D)

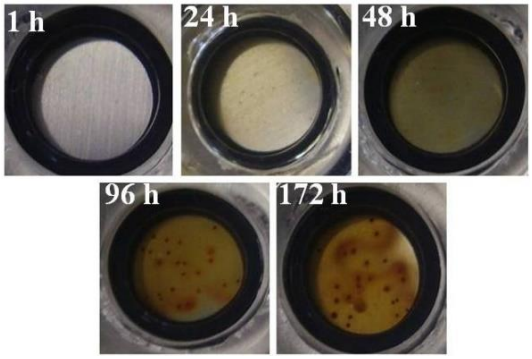

(Figure 5E)

Figure 5. Photos taken after the EIS measurements of samples protected with TEOS / MPTS organic-inorganic hybrid coating with different Ce^{4+} ions

Eclética Química Journal, vol. 44, n. 4, 2019, 27-56
ISSN: 1678-4618
DOI: 10.26850/1678-4618eqj.v44.4.2019.p27-56

concentrations / ppm: (**A**) 0, (**B**) 300, (**C**) 500, (**D**) 700 and (**E**) 900.

In the next paragraphs the influence of Ce^{4+} ions addition in the protective properties of the organic-inorganic hybrid coating will be discussed on the light of the EEC fitting procedures. For the samples protected with the coating doped with 300 to 900 ppm of Ce^{4+} ions the EEC of Fig. 3B adequately fitted the EIS experimental data (Tables 2S-5S, Supplementary data). For this EEC, the time constants at HF (CPE_1//R_1) and LF (CPE_3//R_3) are ascribed to the same phenomena as for the nondoped coating. On the other hand, the time constant at the MF (fitted with the CPE_2//R_2 subcircuit) is attributed to the presence of Ce incorporated into the organic-inorganic hybrid coating, which final oxidation state will be discussed in the second part of this manuscript. Several studies indicated that Ce species added to the hydrolysis solution may form oxides/hydroxides covering part of the metallic surface, and / or complexes located inside the coating, providing greater protection to the substrate[43-45]. Paussa *et al.*[43], using GDOES (glow discharge optical emission spectroscopy) measurements, reported the formation of a Ce compound layer on the substrate surface and inside a ZrO_2 sol-gel coating, improving the corrosion protection provided to the substrate, as verified by EIS experiments. Similar behavior was observed for epoxy coatings modified with pigments used to protect an Al-Zn alloy against corrosion[27]. In this latter case, the impedance data were also fitted using an EEC with three time constants at which the MF one was assigned to the electrical / electrochemical behavior of the pigments present within the coating[27].

For all the coatings doped with Ce^{4+} ions the values of CPE_1-T increase (Table 2S-5S, Supplementary data) and R_1 decrease (Fig. 4A) with immersion time, indicating that the protective properties of the coating are being lost due to electrolyte uptake. These changes occur at different rates depending on the Ce amount added to the hydrolysis solution. Among the studied samples, the one doped with 500 ppm of Ce^{4+} ions showed the slowest changes in these parameters (Table 3S, Supplementary data) when compared to the others. For this particular sample, the capacitive elements CPE_1-T and CPE_2-T slightly increase between 1 h and 408 h of test indicating slow electrolyte uptake by the coating, which seems to maintain its integrity (Fig. 5C), thus avoiding excessive exposure of the substrate to the electrolyte. During this period, R_1 and R_2 values decrease by about one order of magnitude (Fig. 4A and 4B) indicating, respectively, enhanced electrolyte penetration through conductive pathways in the coating and dissolution of Ce ions. For this time span, CPE_3-T decreases (Table 3S, Supplementary data) and R_3 (corresponding to the charge transfer resistance) presents very high values and keeps increasing up to 400 h (Fig. 4C), indicating, respectively, that the reaction rate at the interface is low and that it is progressively hindered. Considering the physical model for the EEC, it is hypothesized that dissolved Ce ions could migrate to cathodic sites precipitating[20,43-45]. The blockage of the cathodic reactions would, consequently, avoid the metal oxidation and, apparently, impart some self-healing properties to the protective coating, as proposed by different authors[46,47].

For longer immersion times (432 h) CPE_1-T increases by approximately one order of magnitude whereas CPE_2-T becomes fifty times higher than at the beginning of the exposure period (Table 3S, Supplementary data). This indicates, respectively, that the protective properties of the coating have been seriously damaged and that much of the Ce ions entrapped within the coating has been dissolved. For this immersion time, visual corrosion of the substrate could be observed, which increased with immersion time (Fig. 5C).

For the other studied samples (doped with 300, 700 or 900 ppm) the same tendencies for the CPE and R were observed, but with higher degradation rates (see Fig. 4A, 4B and 4C, Fig. 5B, 5D and 5E and Tables 2S, 4S and 5S, Supplementary data), and with no clear sign of self-healing properties, which could be ascribed to very defective coatings (note the steep decrease of R_1 (Fig. 4A) and R_2 (Fig. 4B) for these samples). Finally, it must be stressed that, for all investigated samples, α values were between 0.9 and 0.6, indicating heterogeneities in the coating properties and heterogeneous charge distribution on the metallic surface.

Fig. 5 shows photos of the samples surfaces after each EIS measurement. Pitting is observed after 24 h immersion for the samples protected with the organic-inorganic hybrid without and with 300 ppm and 700 ppm of Ce^{4+} ions (Fig. 5A, 5B and 5D). On the other hand, localized corrosion was initiated after 96 h for the coating doped with 900 ppm (Fig. 5E) and after 432 h for the sample prepared with 500 ppm of Ce^{4+} ions (Fig. 5C).

Eclética Química Journal, vol. 44, n. 4, 2019, 27-56
ISSN: 1678-4618
DOI: 10.26850/1678-4618eqj.v44.4.2019.p27-56

These results were highly coherent with the EIS ones confirming that this latter formulation presents the best substrate protection against corrosion. They are also coherent with the thicknesses of the coatings presented in the experimental part.

The sample protected with the modified coating with the best electrochemical response (500 ppm of Ce^{4+} ions) and the unmodified one (reference) were observed by SEM. Fig. 6 presents SEM images of these samples surfaces prior to (A and C) and after (B and D) 240 h immersion in the test electrolyte. Before the corrosion test, the coatings were defect-free and completely covered the substrate surfaces (Fig. 6A and 6C). Before immersion, the maps of elements for these samples (Fig. 2SA and 2SB) show uniform distribution of C, O and Si all over the surface and Fe was not detected. On the other hand, after the completion of the corrosion test, the sample protected by the organic-inorganic hybrid coating without Ce showed cracks distributed throughout the surface (Fig. 6B), indicating a high degree of degradation. This can be attributed both to a low degree of polycondensation and to the hydrolysis of the siloxane bonds due to electrolyte uptake, generating these preferential pathways for the onset of the corrosion process at the substrate surface[25,37] as also detected in the EIS experiments. The EDS microanalysis of this sample after 240 h of test (Fig. 2SC, Supplementary data) showed the presence of iron, especially near the cracks, confirming the existence of preferential corrosion sites. For the sample protected by the coating modified with 500 ppm of Ce^{4+} ions, cracks and surface defects were not observed, even after 240 h of immersion (Fig. 6D), indicating that the integrity of the coating was maintained, corroborating the good EIS results. EDS analysis (Fig. 2SD, Supplementary data) did not identify iron on this sample surface, confirming that the coating acted as an effective barrier, preventing the electrolyte to reach the substrate.

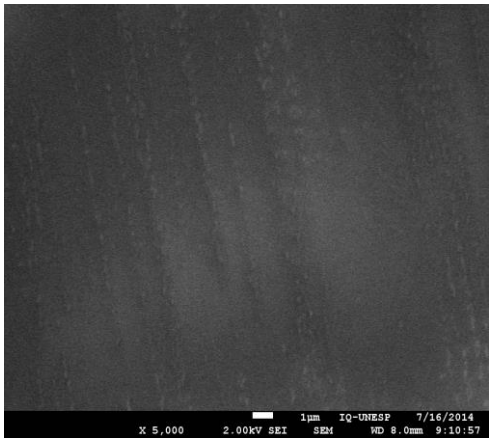

(Figure 6A)

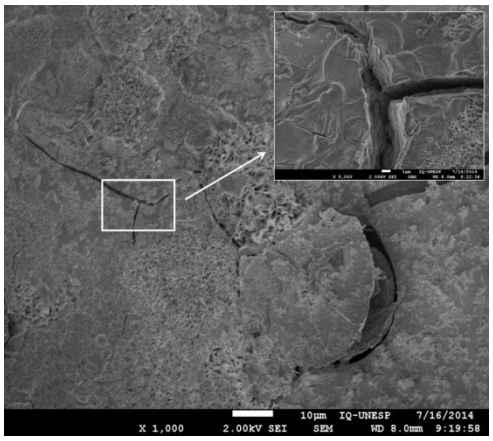

(Figure 6B)

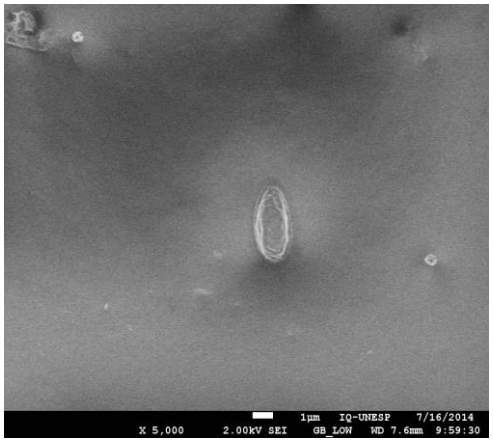

(Figure 6C)

Eclética Química Journal, vol. 44, n. 4, 2019, 27-56
ISSN: 1678-4618
DOI: 10.26850/1678-4618eqj.v44.4.2019.p27-56

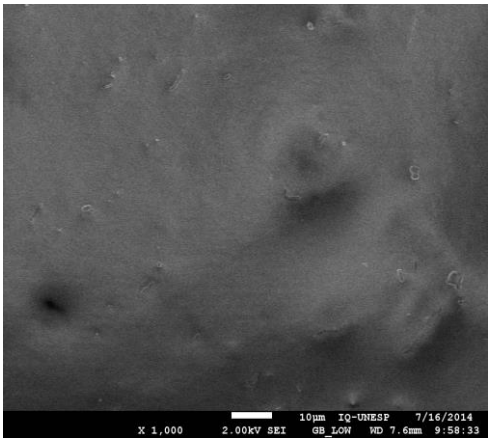

(Figure 6D)

Figure 6. SEM images for the coatings TEOS / MPTS doped with different Ce^{4+} ions concentration / ppm: (**A**) 0 and (**B**) 500 before immersion; (**C**) 0 and (**D**) 500 after 400 h immersion in 0.1 mol L^{-1} NaCl.

3.2. Strategy to identify Ce ions within the organic-inorganic hybrid coating

To make one step ahead in the interpretation of the role of Ce^{4+} ions in the corrosion protection afforded by these organic-inorganic hybrid coatings, it is necessary to have some insight about their effective presence within the coating structure as well as about their oxidation state, which is a complex task considering the low amount of this modifier added to the hydrolysis solution. Only few works[21,45] have detected the presence of Ce in organic-inorganic hybrid coating, but its amount needs to be, in general, higher than that used in the present investigation. Paussa *et al.*[43], using GDOES measurements, reported the presence of a thin Ce layer on the substrate surface and inside the ZrO_2 coating. Cerium (III) and cerium (IV) species were detected in polysiloxane hybrid by the deconvolution of the complex Ce 3d spectrum of the XPS analysis[20,21]. In general, the main problem for the XPS analysis is the amount of Ce ions in the sample, lower than the detection limit of the equipment. In addition, photooxidation of Ce ions during XPS measurements has also been reported[21]. Therefore, attempting to assess/identify the presence of Ce ions in the organic-inorganic hybrid coating, XPS, LIBS and UV-Vis techniques were used.

Figs. 7 and 8 show, respectively, the XPS spectra for the C1s, O1s and Si2p for samples coated with the organic-inorganic hybrid coating without and with 500 ppm of Ce^{4+} ions. Table 1 shows the binding energy values, peak areas and full width at half-maximum (FWHM) determinations. In the Si2p (Fig. 7C and 8C) and O1s (Fig. 7B and 8B) spectra, it is important to highlight the presence of two peaks that characterize the siloxane (Si-O-Si) structure and the polycondensation degree of the organic-inorganic hybrid coating[48-51]. The first peak in the O1s spectrum (≈ 533 eV) is assigned to the oxygen-silicon (Si-O-Si) bond; the second peak in the Si2p spectrum, at 103.7 eV, is related to the formation of connection strings (SiO_2) in the organic-inorganic hybrid structure[46-49]. However, the distortion in the SiO_2 binding energy was not accessed, the difference between dopant-modified and unmodified coatings is within the experimental error (Table 1), probably because the low Ce^{4+} ions concentration. But the peak intensity at 103.7 eV for both coatings can be compared: for the doped coating (Fig. 8), the intensity of this peak was 3.5%, a slightly higher value than that to the nondoped coating, suggesting an increase in the polycondensation degree of the organic-inorganic hybrid coating[20,48,50]. A comparison of the effect of Ce obtained in this work with that of literature[20,50] is impaired, since dopant concentration is ~15x smaller. This structure extends throughout the material, resulting in a denser and more effective barrier against corrosion, supporting the results of microscopic analyses and electrochemical measurements. For the C1s (Fig. 7A and 8A) spectra different chemical environments were observed for both samples. The coating without the dopant shows two sharp peaks at 285 eV and 287 eV related, respectively, to alkyl CCH and C-O structure connections, whereas for the doped sample only the peak at 285 eV is sharp, the other one is quite smooth and low. This different chemical environment for the nondoped sample can be attributed to a lower polycondensation degree of the organic-inorganic hybrid structure and/or to the presence of a larger amount of organic phase incorporated to the organic-inorganic hybrid structure. The presence of Ce ions was not detected in the XPS measurements, probably because its amount within the coating is lower than the detection limit of the equipment. In some studies, spectra resolved for Ce were only possible with the use of quantities greater than 1000 ppm[19,21]. For the same reason LIBS measurements were unsuccessful in detecting Ce in the coating composition when concentrations below 1000 pm were used.

Eclética Química Journal, vol. 44, n. 4, 2019, 27-56
ISSN: 1678-4618
DOI: 10.26850/1678-4618eqj.v44.4.2019.p27-56

Table 1. Results of fitting XPS spectra for samples protected with the organic-inorganic hybrid coating with 0 and 500 ppm of Ce(IV). Estimated error in areas is lower than 2.5%.

	0 ppm			500 ppm		
	BE	**FHWM**	**Area**	**BE**	**FHWM**	**Area**
C1s	284.9	1.67	59.36	284.9	1.57	62.72
	286.2	2.00	14.02	286.6	1.56	32.34
	288.8	1.70	14.21	288.2	1.29	3.21
	289.0	1.73	12.42	289.3	1.30	1.73
O1s	530.7	1.42	3.18	530.7	1.41	2.32
	532.5	1.71	83.07	532.7	1.71	92.83
	533.7	1.94	13.76	534.1	1.87	4.84
Si2p	102.6	1.68	27.68	102.4	1.56	25.17
	103.3	1.81	72.32	103.4	1.90	74.83

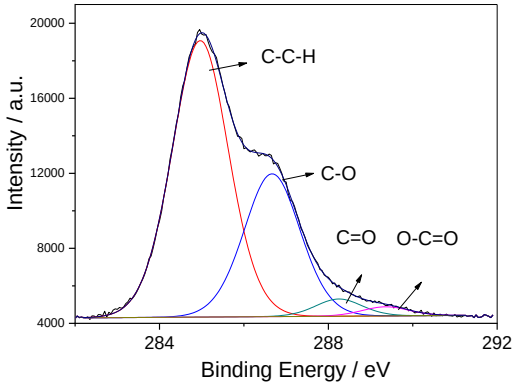

(Figure 7A)

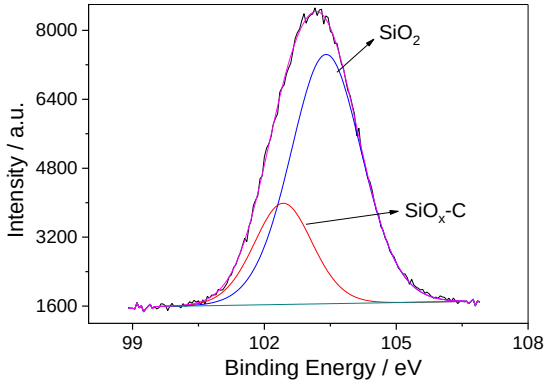

(Figure 7B)

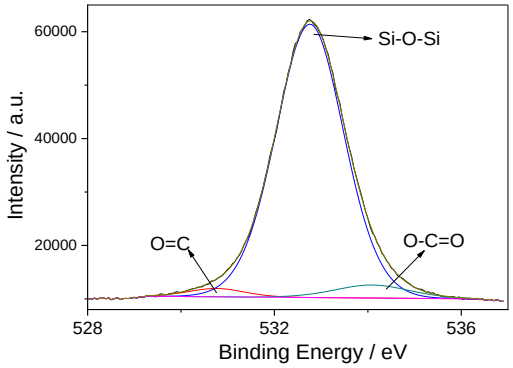

(Figure 7C)

Figure 7. X-ray photoelectron spectra for the C1s, O1s and Si2p for the organic-inorganic hybrid coating without Ce^{4+} ions: (**A**) C 1s, (**B**) O 1s and (**C**) Si 2p.

Eclética Química Journal, vol. 44, n. 4, 2019, 27-56
ISSN: 1678-4618
DOI: 10.26850/1678-4618eqj.v44.4.2019.p27-56

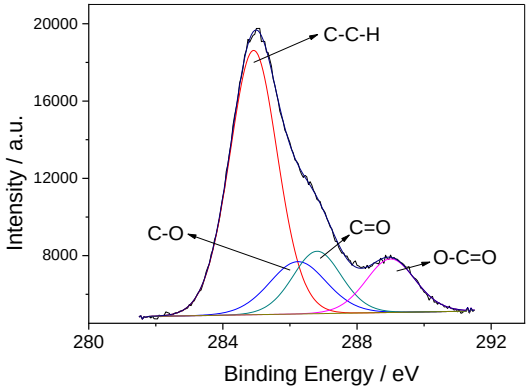

(Figure 8A)

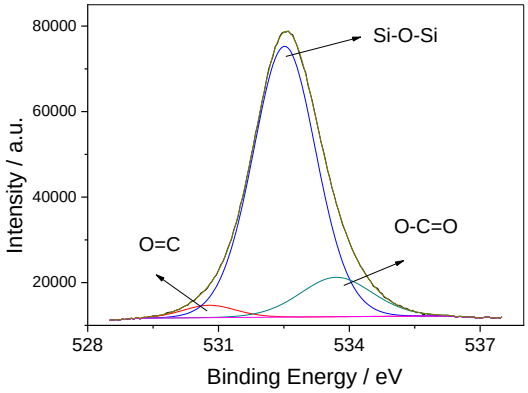

(Figure 8B)

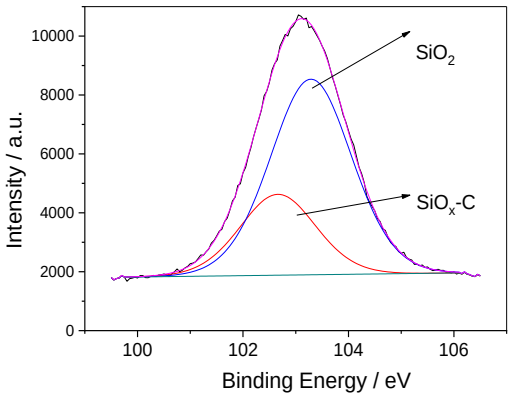

(Figure 8C)

Figure 8. X-ray photoelectron spectra for the C1s, O1s and Si2p for the organic-inorganic hybrid coating doped with 500 ppm of **Ce^{4+}** ions (**A**) C 1s, (**B**) O 1s and (**C**) Si 2p.

Fig. 9 shows LIBS spectra for the coatings without and with 1500 ppm of Ce^{4+} ions prepared in the same conditions as those previously reported (*subsection 2.2*) and deposited onto copper substrate to avoid the strong interference of iron in Ce analysis[24]. To improve the sensibility for Ce detection, one spectrum was obtained with a shearing system that increases the atomization process. The main lines at 570 nm and 590 nm observed in spectra of Fig. 9A and 9B can be attributed to Si and the lines at 594 nm (Fig. 9C) and 428 nm (Fig. 9D) are attributed to Ce[24], confirming the presence of this specie within the coating structure.

Eclética Química Journal, vol. 44, n. 4, 2019, 27-56
ISSN: 1678-4618
DOI: 10.26850/1678-4618eqj.v44.4.2019.p27-56

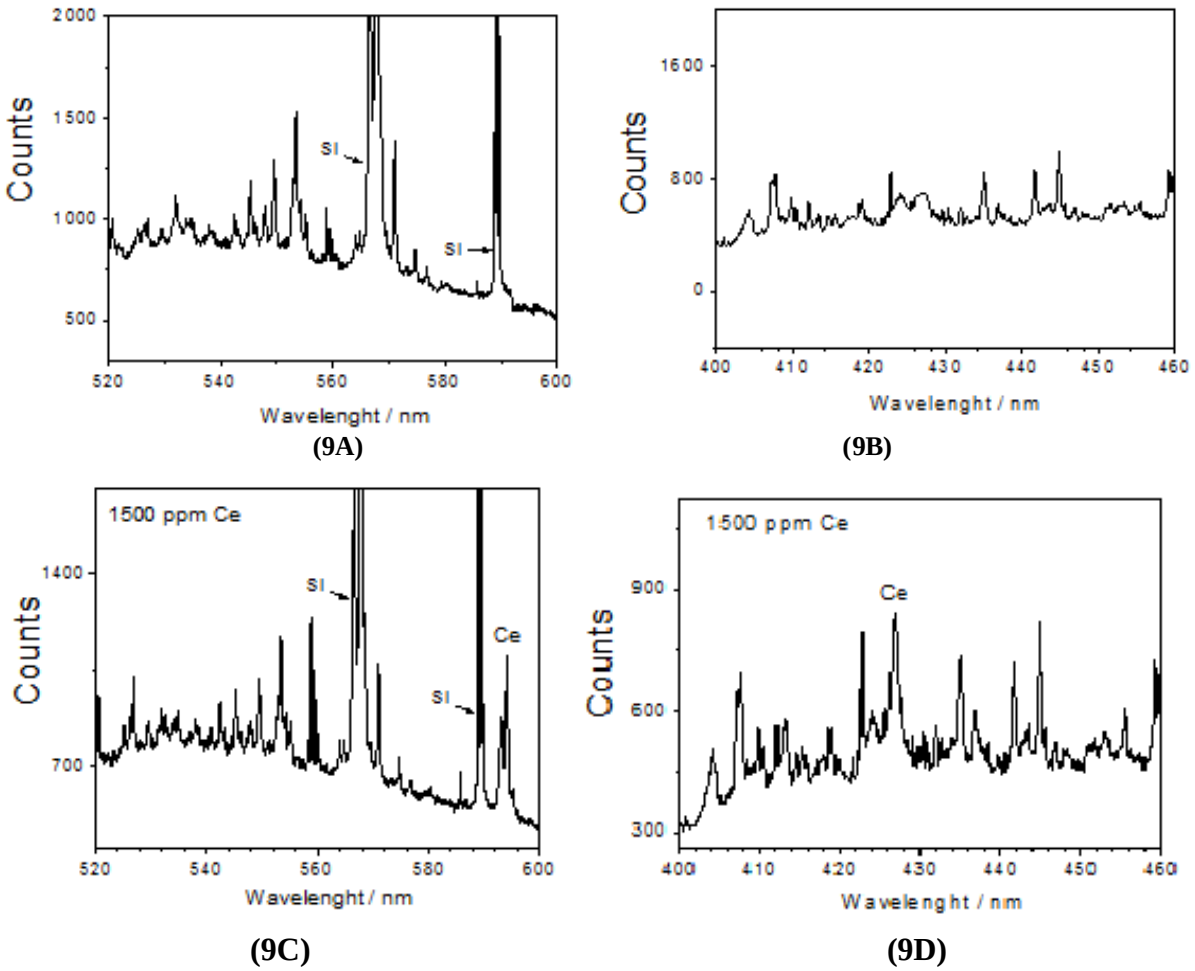

Figure 9. LIBS spectra obtained for pellets of free-standing organic-inorganic hybrid coating nondoped (**A**) and (**B**). Doped with 1500 ppm of Ce^{4+} ions (**C**) and (**D**).

Fig. 10 shows the UV-Vis spectra of cerium (III) nitrate, cerium (IV) sulfate aqueous solutions, and of Ce ions extraction from freestanding coating doped with 500 ppm of cerium (III) or cerium (IV) salts in naturally aerated deionized water (pH 6.5). Two main relatively wide bands were observed at around 280 nm and 250 nm attributed to the charge transfer transition from oxygen to the d-Ce(IV) orbital and to f-d Ce(III) transition, respectively[52,53]. Three main information are highlighted from these spectra: (**a**) Ce is present inside the doped freestanding coating and can be at least partially extracted with water, indicating that a certain amount of Ce is probably not strongly bonded to the organic molecules of the organic-inorganic hybrid coating; (**b**) Ce is mainly in the cerium (IV) oxidation state regardless if the doped coating were prepared using cerium (III) or cerium (IV) salts; (**c**) a small amount of cerium (IV) species is present in the cerium (III) nitrate salt.

Eclética Química Journal, vol. 44, n. 4, 2019, 27-56
ISSN: 1678-4618
DOI: 10.26850/1678-4618eqj.v44.4.2019.p27-56

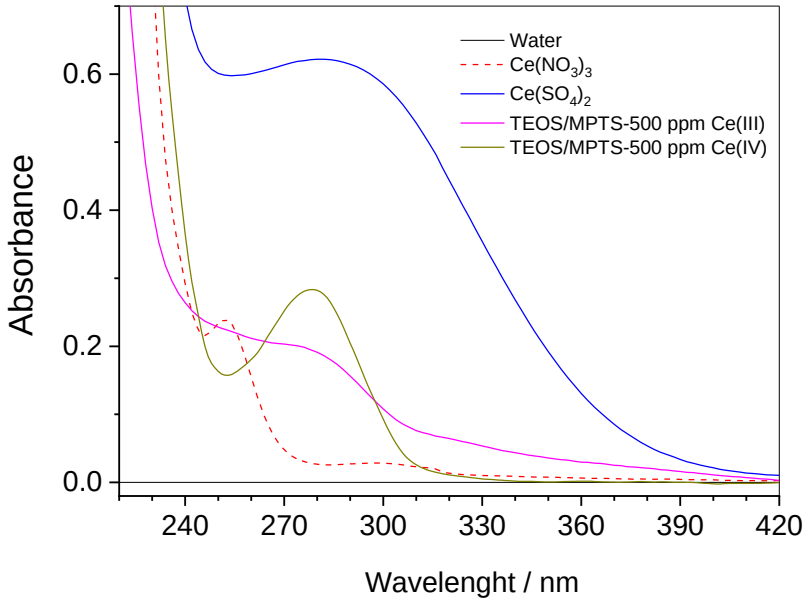

Figure 10. UV-Vis spectra of aqueous solution containing cerium (III) nitrate, cerium (IV) sulfate and solutions of cerium ions extraction, in the presence of oxygen, from the coating doped with 500 ppm of cerium (III) or cerium (IV) salts.

UV-Vis spectra were also obtained for aqueous solution resulting from Ce ions extraction from the organic-inorganic hybrid coating doped with different amounts of cerium (IV) species (Fig. 3S, Supplementary data). From these spectra, the intensity of the peaks follows the order: 900 ppm > 500 ppm > 300 ppm, indicating that the quantity of Ce ions extracted is proportional to its content in the doped coating. To have an idea about the amount of Ce^{4+} ions extracted from the freestanding coating, an analytical curve was constructed for Ce^{4+} ions (Fig. 4S, Supplementary data), the result was a straight line indicating that the amount of Ce ions liberated from the doped coating is proportional to its amount in the doped coating. Sequentially, 3 g of freestanding doped coating (TEOS / MPTS with 500 ppm cerium (IV) ions) was immersed in 3 mL of purified water (pH 6.5) and after extracting for 15 days, the solution was filtered and analyzed by UV-Vis spectrophotometry. The absorbance of the filtered solution was 0.27 corresponding to 35 ppm of Ce^{4+} ions, which means 35 μg cerium (IV) / g of freestanding doped coating. Based on the nominal composition, the free-standing doped coating has 654 μg cerium (IV) / g, which means that around only 5% of Ce was extracted from the coating. These results also confirm that such amount of Ce is almost impossible to be detected by XPS or LIBS techniques.

Considering that the solution of Ce ions extracted from the freestanding coating doped with cerium (III) salt also showed the band at around 280 nm with similar shape to that acquired from the coating doped with Ce^{4+} ions, extraction of Ce ions from doped coating was performed in inert atmosphere by bubbling purified argon into the water before and during extraction (Fig. 11). For these experiments, the solution obtained by extracting Ce ions from the freestanding coating doped with cerium (III) salt shows a band at around 254 nm (characteristic of Ce^{3+} ions) and a stronger band at around of 276 nm characteristic of Ce^{4+} ions. However, for the solution obtained from the coating doped with cerium (IV) salt, only the band attributed to cerium (IV) was observed. This result suggests that, in both doped coating, Ce is mainly present as cerium (IV) species.

Eclética Química Journal, vol. 44, n. 4, 2019, 27-56
ISSN: 1678-4618
DOI: 10.26850/1678-4618eqj.v44.4.2019.p27-56

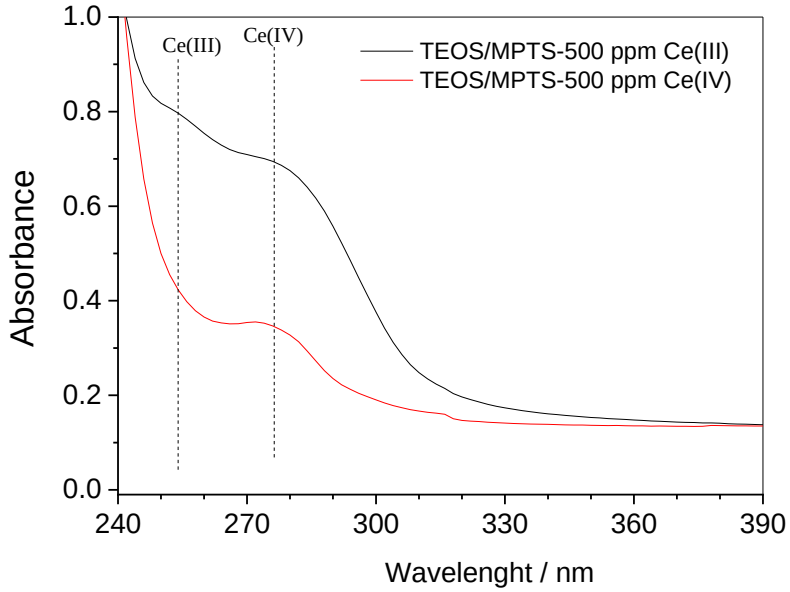

Figure 11. UV-Vis spectra of aqueous solutions of cerium ions extraction in the absence of oxygen from the coating doped with 500 ppm of cerium (III) or cerium (IV) salts.

For comparison with the experiments performed with the extraction from the freestanding coating doped with cerium, UV-Vis measurements were performed with solid organic-inorganic hybrid coating deposited onto glass (Fig. 5S, Supplementary data). For organic-inorganic hybrid coating doped with cerium (IV) ions and with cerium (III) ions one relatively wide band was observed in the range of 250 - 270 nm. In the similar wavelength range one band was observed and assigned to the UV-Vis spectrum of the $Ce(SO_4)_2$ crystals. Therefore, for the coating, Ce is mainly in the cerium (IV) oxidation state regardless if the doped coating was prepared using cerium (III) or cerium (IV) salts.

The results reported above indicated that cerium (IV) species react with ethanol and accelerate the radical formation and the polymerization process to form the organic-inorganic hybrid coating. Therefore, it would be expected a spectrum characteristic of cerium (III) species when the cerium was extracted from the doped coatings. Surprisingly, the main species observed in the extracted solution was cerium (IV) species independent on the oxidation state of the Ce ions added to the hydrolysis solution. The presence of cerium (IV) species into the lixiviated solution can be explained admitting the oxidation of cerium (III) to cerium (IV) species in the presence of oxygen, according to the equations[52,53]:

$$4Ce(OH)^{2+} + O_2 + 2H_2O \rightarrow 4Ce(OH)_2^{2+} \quad (1)$$

$$4Ce^{3+} + O_2 + 6H_2O \rightarrow 4Ce(OH)_2^{2+} + 4H^+ \quad (2)$$

$$4Ce^{3+} + O_2 + 14H_2O \rightarrow 4Ce(OH)_4 + 12H^+ \quad (3)$$

$$4Ce^{3+} + O_2 + 6H_2O \rightarrow 4CeO_{2(precip)} + 12H^+ \quad (4)$$

AFM analysis (Fig. 6S) reinforces the presence of cerium (IV) inside the TEOS/MPTS organic-inorganic hybrid coating as following: an uniform and homogeneous surface without the presence of precipitates is observed for the organic-inorganic hybrid coating modified with cerium (IV) ions (Fig. 6SA, Supplementary data), while a surface with small precipitates at metal surface, possibly cerium oxides / hydroxides, is observed for the organic-inorganic hybrid coating doped with Ce^{3+} ions (Fig. 6SB, Supplementary data).

Trabelsi *et al*.[9] have studied the effect of cerium (III)-doping of silane solutions in the protection of galvanized steel and also observed cerium (IV) species formation. Several possibilities can explain the presence of cerium (IV) species: (a) oxidation of $Ce(OH)_3$ to CeO_2 as consequence of the

Eclética Química Journal, vol. 44, n. 4, 2019, 27-56
ISSN: 1678-4618
DOI: 10.26850/1678-4618eqj.v44.4.2019.p27-56

corrosion reactions caused by anodic areas formation on the steel surface; (b) generation of hydrogen peroxide as consequence of the oxygen reduction during cathodic reaction; (c) in solution oxidation of Ce^{3+} ions to $Ce(OH)_2^{2+}$ ions and further precipitation of CeO_2; (d) dismutation solid state reaction of $Ce(OH)_3$ to form CeO_2 and (e) a possible oxidation of Ce^{3+} ions to Ce^{4+} ions inside the film.

According to a parallel study of the cerium ions effect on the precursor solutions, Ce^{4+} ions would be reduced to Ce^{3+} ions during the polymerization redox reaction to form organic-inorganic coating (Fig. 1S, Supplementary data), and a fraction of Ce^{3+} ions could be re-oxidized to Ce^{4+} ions via one or more reactions represented in Eq. 1-4. The Ce^{4+} and Ce^{3+} ions may be trapped inside the coating and, as the coating may undergo some hydrolysis in contact with water / electrolyte, these ions are released / lixiviated from the coating and detected by the UV-Vis analysis. This process is reinforced by the AFM results described above. Therefore, Ce^{4+} ions may be present in the as-prepared organic-inorganic hybrid coating as trapped-like species. Briefly, it is proposed that part of Ce species present in the doped organic-inorganic hybrid coating is relatively free or trapped within the coating structure as soluble and can be partially removed by extraction with water or partial hydrolysis of the coating.

4. Conclusions

The influence of the addition of Ce^{4+} ions to the hydrolysis solution on the protective properties of a TEOS / MPTS organic-inorganic hybrid coating was investigated. The results demonstrated that when added at an appropriate amount (in the present case 500 ppm) the dopant can greatly improve the barrier and protective properties of the organic-inorganic hybrid coating, as demonstrated by EIS results.

XPS measurements have shown that the improvement of the barrier properties of the coating can be ascribed to the formation of a denser siloxane (Si-O-Si) network in the presence of cerium (IV) ions.

An experimental strategy designed using LIBS have evidenced the presence of Ce ions within the coating structure, whereas UV-Vis experiments evidenced that Ce is mainly present in the (IV)-oxidation state.

A mechanism was proposed where cerium (III) ions from the redox polymerization reaction may be oxidized back to cerium (IV) species mainly by the presence of oxygen.

6. Acknowledgements

The authors would like to thank CNPq (Process 305890/2010-7) and CAPES (Fernando Santos da Silva social demand scholarship). The authors thank Prof. Dr. Fabíola M. Verbi Pereira for her collaboration in the LIBS analysis and results interpretation.

7. References

[1] Hammer, P., dos Santos, F. C., Cerrutti, B. M., Pulcinelli, S. H., Santilli, C. V., Carbon nanotube-reinforced siloxane-PMMA hybrid coatings with high corrosion resistance, Prog. Org. Coat. 76 (4) (2013) 601-608. https://doi.org/10.1016/j.porgcoat.2012.11.015.

[2] Brinker, C. J., Scherer G. W. Sol-Gel Science The Physics and Chemistry processing, Academic Press, San Diego 1 (1990) 912. https://www.elsevier.com/books/sol-gel-science/brinker/978-0-08-057103-4.

[3] Schubert, U., Husing, N., Lorenz, A., Hybrid Inorganic-Organic Materials by Sol-Gel Processing of Organofunctional Metal Alkoxides, Chem. Mater. 7 (11) (1995) 2010-2027. https://doi.org/10.1021/cm00059a007.

[4] Lamaka, S. V., Montemor, M. F., Galio, A. F., Zheludkevich, M. L., Trindade, C., Dick, L. F., Ferreira, M. G. S., Novel hybrid sol–gel coatings for corrosion protection of AZ31B magnesium alloy, Electrochim. Acta 53 (14) (2008) 4773-4783. https://doi.org/10.1016/j.electacta.2008.02.015.

[5] Van Ooij, W. J., Zhu, D., Stacy, M., Seth, A., Mugada, T., Gandhi, J., Puomi, P., Corrosion Protection Properties of Organofunctional Silanes-An Overview, Tsinghua Sci. and Technol. 10 (6) (2005) 639-664. https://doi.org/10.1016/S1007-0214(05)70134-6.

[6] Kron, J., Deichmann, K. J, Rose, K., Self-healing properties of new surface treatments, European Federation of Corrosion Publications, London, 2010. ISBN-13: 978-1906540364.

[7] Wang, D., Bierwagen, G. P., Sol–gel coatings on metals for corrosion protection, Prog. Org. Coat. 64 (4) (2009) 327-338. https://doi.org/10.1016/j.porgcoat.2008.08.010.

[8] Ferreira, M. G. S., Duarte, R. G. Montemor, M. F., Simões, A. M. P., Silanes and rare earth salts as chromate replacers for pre-treatments on galvanised steel, Electrochim. Acta 49 (17, 18) (2004) 2927-2935. https://doi.org/10.1016/j.electacta.2004.01.051.

[9] Trabelsi, W., Cecilio, P., Ferreira, M. G. S., Montemor, M. F., Electrochemical assessment of the self-healing properties of Ce-doped silane solutions for the pre-treatment of galvanized steel substrates, Prog. Org. Coat. 54 (4) (2005) 276-284. https://doi.org/10.1016/j.porgcoat.2005.07.006.

[10] Montemor, M. F., Ferreira, M. G. S., Cerium salt activated nanoparticles as fillers for silane films: Evaluation of the corrosion inhibition performance on galvanised steel substrates, Electrochim. Acta 52 (24) (2007) 6976-6987. https://doi.org/10.1016/j.electacta.2007.05.022.

[11] Ozturk, T., Cakmak, I., Synthesis of block copolymers via redox polymerization: a critical review, Iranian Polym. J. 16 (8) (2007) 561-581. http://journal.ippi.ac.ir/manuscripts/IPJ-2007-10-2427.pdf.

[12] Nagarajan, S., Srinivason, K. S. V., Block copolymerization initiated by Ce(IV)- poly(ethylene glycol) redox system-kinetics and characterization, Europe Polym. J. 30 (1) (1994) 113-119. https://doi.org/10.1016/0014-3057(94)90240-2.

[13] Fernanderz, M. D., Fernandez, M. J, Guzman, G. M., Study of the morphology of poly(methyl methacrylate) as polymerized by the redox system Ce(IV)–isopropyl alcohol, J. Polym. Sci. 27 (10) (1989) 3439-3450. https://doi.org/10.1002/pola.1989.080271022.

[14] Cho, U. Y., Romero, J. R., Chemical and electrochemical oxidative dimerization of carbonyl compounds by cerium(IV) salts. A comparative study, Tetr. Lett. 36 (48) (1995) 8757-8760. https://doi.org/10.1016/0040-4039(95)01921-4.

[15] Cho, L. Y., Madurro, J. M., Romero, J. R., Electrooxidation of β-Dicarbonyl Compounds Using Ceric Methanesulfonate as Mediator: Some Kinetics and Spectroscopic Studies, J. Cat. 186 (1) (1999) 31- 35. https://doi.org/10.1006/jcat.1999.2541.

[16] Purgato, F. L. S., Romero, J. R., Electrooxidation of Hydroxyl Compounds Using Cerium Salts as Mediators: The Importance of Substrate Size for Catalyst Regeneration, Journal of Catalysis 209 (2) (2002) 394-400. https://doi.org/10.1006/jcat.2002.3646.

[17] Aleixo, P. C., Cho, L. Y., Romero, J. R., Oxygen as an Oxidizing Agent in Electrocatalytic Oxidation of β-Dicarbonylic Compounds Using Ce^{IV} as a Mediator, J. of Cat. 192 (1) (2000) 248-251. https://doi.org/10.1006/jcat.2000.2829.

[18] Lofrano, R. C. Z., Madurro, J. M., Romero, J. R., Preparation and properties of an electrode coated with a cerium poly(allyl ether p-benzenesulfonate) film for electroorganic reactions, J. Mol. Catal. A: Chem. 153 (1, 2) (2000) 237-242. https://doi.org/10.1016/S1381-1169(99)00354-4.

[19] Suegama, P. H., de Melo, H. G., Benedetti, A. V., Aoki, I. V., Influence of cerium (IV) ions on the mechanism of organosilane polymerization and on the improvement of its barrier properties, Electrochim. Acta 54 (9) (2009) 2655-2662. https://doi.org/10.1016/j.electacta.2008.11.007.

[20] Palomino, L. M., Suegama, P. H., Aoki, I. V., Montemor, M. F., de Melo H. G., Electrochemical study of modified cerium–silane bi-layer on Al alloy 2024-T3, Corr. Sci. 51 (6) (2009) 1238-1250. https://doi.org/10.1016/j.corsci.2009.03.012.

[21] Hammer, P., Schiavetto, M. G., Santos, F. C., Benedetti, A. V., Pulcinelli, S. H., Santilli, C. V., Improvement of the corrosion resistance of polysiloxane hybrid coatings by cerium doping, J. Non-Cryst. Solids 356 (44, 49) (2010) 2606-2612. https://doi.org/10.1016/j.jnoncrysol.2010.05.013.

[22] Suegama, P. H., Sarmento, V. H. V., Montemor, M. F., Benedetti, A. V., de Melo, H. G., Aoki, I. V., Santilli, C. V., Effect of cerium (IV) ions on the anticorrosion properties of siloxane-poly (methyl methacrylate) based film applied on tin coated steel, Electrochim. Acta 55 (18) (2010) 5100-5109. https://doi.org/10.1016/j.electacta.2010.04.002.

[23] Orazem, M. E., Tribollet, B., Electrochemical Impedance Spectroscopy, John Wiley & Sons, New Jersey, 1st ed., 2008. ISBN: 111820994X.

[24] Phuoc, T. X., Wang, P., McIntyre, D., Detection of rare earth elements in Powder River Basin sub-bituminous coal ash using laser-induced breakdown spectroscopy (LIBS), Fuel 163 (1) (2016) 129-132. https://doi.org/10.1016/j.fuel.2015.09.034.

[25] Geenen, F. M., de Wit, J. H. W., An impedance spectroscopy study of the degradation mechanism for a model epoxy coating on mild steel, Prog. Org. Coat. 18 (3) (1990) 299-312. https://doi.org/10.1016/0033-0655(90)80007-L.

Eclética Química Journal, vol. 44, n. 4, 2019, 27-56
ISSN: 1678-4618
DOI: 10.26850/1678-4618eqj.v44.4.2019.p27-56

[26] Sarmento, V. H. V, Schiavetto, M. G., Hammer, P., Benedetti, A. V., Fugivara, C. S., Suegama, P. H, Pulcinelli S. H., Santilli C. V., Corrosion protection of stainless steel by polysiloxane hybrid coatings prepared using the sol–gel process, Surf. & Coat. Technol. 204 (16, 17) (2010) 2689-2701. https://doi.org/10.1016/j.surfcoat.2010.02.022.

[27] Bonora, P. L., Deflorian, F., Fedrizzi, L., Electrochemical impedance spectroscopy as a tool for investigating underpaint corrosion, Electrochim. Acta 41 (7, 8) (1996) 1073-1082. https://doi.org/10.1016/0013-4686(95)00440-8.

[28] Pepe, A., Aparicio, M., Duran, A., Cere, S., Cerium hybrid silica coatings on stainless steel AISI 304 substrate, J. Sol-Gel Sci. Techn. 39 (2) (2006) 131-138. https://doi.org/10.1007/s10971-006-9173-1.

[29] Yaggi, C., Yildiz, U., Redox polymerization of methyl methacrylate with allyl alcohol 1,2-butoxylate-block-ethoxylate initiated by Ce (IV)/HNO_3 redox system, Europe Poly. J. 41 (1) (2005) 177-184. https://doi.org/10.1016/j.eurpolymj.2004.08.008.

[30] Capelossi, V. R., Aoki, I. V., Influence of sonication on anticorrosion properties of a sulfur silane film dopped with Ce (IV) on galvannealed steel, Prog. Org. Coat. 76 (5) (2013) 812-820. https://doi.org/10.1016/j.porgcoat.2013.01.012.

[31] Molander, G. A., Application of lanthanide reagents in organic synthesis, Chem. Rev. 92 (1) (1992) 29-68. https://doi.org/10.1021/cr00009a002.

[32] Choi, Y-S., Nesic, S., Ling, S., Effect of H_2S on the CO_2 corrosion of carbon steel in acidic solutions, Electrochim. Acta 56 (4) (2011) 1752-1760. https://doi.org/10.1016/j.electacta.2010.08.049.

[33] Keddam, M., Mattos, O. R. Takenouti H., Reaction Model for Iron Dissolution Studied by Electrode Impedance: II. Determination of the Reaction Model, J. Electrochem. Soc. 128 (2) (1981) 266-274. https://doi.org/10.1149/1.2127402.

[34] Keddam, M., Mattos, O. R., Takenouti, H., Reaction Model for Iron Dissolution Studied by Electrode Impedance I. Experimental Results and Reaction Model, J. Electrochem. Soc. 128 (1) (1981) 257-266. http://jes.ecsdl.org/content/128/2/257.short.

[35] Epelboin, I., Keddam, M., Mattos, O. R., Takenouti, H., The dissolution and passivation of Fe and Fe-Cr alloys in acidified sulphate medium: Influences of pH and Cr content, Corr. Sci. 19 (12) (1979) 1105-1112. https://doi.org/10.1016/S0010-938X(79)80128-6.

[36] Zhu, D., van Ooij, W. J., Corrosion protection of metals by water-based silane mixtures of bis-[trimethoxysilylpropyl]amine and vinyltriacetoxysilane, Prog. Org. Coat. 49 (1) (2004) 42-53. https://doi.org/10.1016/j.porgcoat.2003.08.009.

[37] van Westing, E. P. M., Ferrari, G. M., de Wit, J. H. W., The determination of coating performance with impedance measurements-III. *in situ* determination of loss of adhesion, Corros. Sci. 36 (6) (1994) 979-994. https://doi.org/10.1016/0010-938X(94)90198-8.

[38] Musiani, M., Orazem, M. E., Pébère, N., Tribollet, B., Vivier, V., Constant-Phase-Element Behavior Caused by Coupled Resistivity and Permittivity Distributions in Films, J. Electrochem. Soc. 158 (12) (2011) C424-C428. https://doi.org/10.1149/2.039112jes.

[39] Hirschorn, B., Orazem, M. E., Tribollet, B., Vivier, V., Frateur, I., Musiani, M. J., Constant Phase-Element Behavior Caused by Resistivity Distributions in Films I. Theory, J. Electrochem. Soc. 157 (12) (2010) C452-C457. https://doi.org/10.1149/1.3499564.

[40] Hirschorn, B., Orazem, M. E., Tribollet, B., Vivier, V., Frateur, I., Musiani, M., Constant Phase-Element Behavior Caused by Resistivity Distributions in Films II. Applications, J. Electrochem. Soc. 157 (12) (2010) C458-C563. https://doi.org/10.1149/1.3499565.

[41] Sakai, R. T., di L Cruz, F. M., de Melo, H. G., Benedetti, A. V., Santilli, C. V., Suegama, P. H., Electrochemical study of TEOS, TEOS/MPTS, MPTS/MMA and TEOS/MPTS/MMA films on tin coated steel in 3.5% NaCl solution, Prog. Org. Coat. 74 (2) (2012) 288-381. https://doi.org/10.1016/j.porgcoat.2012.01.001.

[42] van Westing, E. P. M., Ferrari, G. M., de Witt, J. H. W., The determination of coating performance with impedance measurements-II. Water uptake of coatings, Corros. Sci. 36 (6) (1994) 957-977. https://doi.org/10.1016/0010-938X(94)90197-X.

[43] Paussa, L., Rosero-Navarro, N. C., Bravin, D., Andreatta, F., Lanzutti, A., Aparicio, M., Durán, A., Fedrizzi, L. ZrO_2 sol-gel pre-treatments doped with cerium nitrate for the corrosion protection of AA6060, Prog. Org. Coat. 74 (2) (2012) 311-319. https://doi.org/10.1016/j.porgcoat.2011.08.017.

[44] Silva, F. S., Suegama, P. H., Silva, W. P., Rinaldi, A. W., Domingues, N. L. C., Matsumoto, M. Y., Salazar, L. G., Effect of Different Dopants in Films TEOS/MPTS Used to Protect the Carbon Steel, Mater. Sci. Forum 805 (2015) 167-171.

Eclética Química Journal, vol. 44, n. 4, 2019, 27-56
ISSN: 1678-4618
DOI: 10.26850/1678-4618eqj.v44.4.2019.p27-56

https://doi.org/10.4028/www.scientific.net/MSF.805.167.

[45] Arnott, D. R., Ryan, N. E., Hinton, B. R. W., Auger and XPS studies of cerium corrosion inhibition on 7075 aluminum alloy, Applic. of Surf. Sci. 22-23 (1) (1985) 236-251. https://doi.org/10.1016/0378-5963(85)90056-X.

[46] Rosero-Navarro, N. C., Pellice, S. A., Duran, A., Aparicio, M., Effects of Ce-containing sol–gel coatings reinforced with SiO_2 nanoparticles on the protection of AA2024, Corr. Sci. 50 (5) (2008) 1283-1291. https://doi.org/10.1016/j.corsci.2008.01.031.

[47] Naderi, R., Fedel, M., Deflorian, F., Poelman, M., Olivier, M., Synergistic effect of clay nanoparticles and cerium component on the corrosion behavior of eco-friendly silane sol–gel layer applied on pure aluminum, Surf. & Coat. Technol. 224 (15) (2013) 93-100. https://doi.org/10.1016/j.surfcoat.2013.03.005.

[48] Nocun, M., Cholewa-Kowalska, K., Łaczka, M., Structure of hybrids based on TEOS cyclic forms of siloxane system, J. Mol. Struct., 938 (1-3) (2009) 24-28. https://doi.org/10.1016/j.molstruc.2009.08.034.

[49] Materne, T., de Buyl, F., Witucki, G. L., Organisilane technology in coating applications, Dow Corning, Midland, 1st ed., 2004.

[50] Montemor, M. F., Ferreira, M. G. S., Analytical and microscopic characterisation of modified bis-[triethoxysilylpropyl] tetrasulphide silane films on magnesium AZ31 substrates, Prog. Org. Coat. 60 (3) (2007) 228-237. https://doi.org/10.1016/j.porgcoat.2007.07.019.

[51] Tabata, A., Fujii, S., Suzuoki, Y., Mizutani, T., Ieda, M., X-ray photoelectron spectroscopy (XPS) of hydrogenated amorphous silicon carbide (a-Si_xC_{1-x}:H) prepared by the plasma CVD method, J. Phys. D: Appl. Phys. 23 (3) (1990) 316-320. https://doi.org/10.1088/0022-3727/23/3/008.

[52] Scott, H. A., Yu, P., O'Keefe, T. J., O'Keefe, M. J., Stoffer, J. O., The Phase Stability of Cerium Species in Aqueous Systems I. E-pH Diagram for the Ce-HClO4-H2OCe-HClO4-H2O System, J. Electrochem. Soc. 149 (2002) C623-C630. https://doi.org/10.1002/chin.200309018.

[53] Yu, P., Scott, H. A., O'Keefe, T. J., O'Keefe, M. J., Stoffer, J. O., The Phase Stability of Cerium Species in Aqueous Systems II. The Formula Systems. Equilibrium Considerations and Pourbaix Diagram Calculations, J. Electrochem. Soc. 153 (1) (2006) C74-C79. https://doi.org/10.1149/1.1516775

Eclética Química Journal, vol. 44, n. 4, 2019, 27-56
ISSN: 1678-4618
DOI: 10.26850/1678-4618eqj.v44.4.2019.p27-56

Supplementary data

Influence of Ce(IV) ions amount on the electrochemical behavior of organic-inorganic hybrid coatings in 0.1 mol L^{-1} NaCl solution

Figure 1S shows the Nyquist plots for coated samples containing different amounts of Ce(IV).

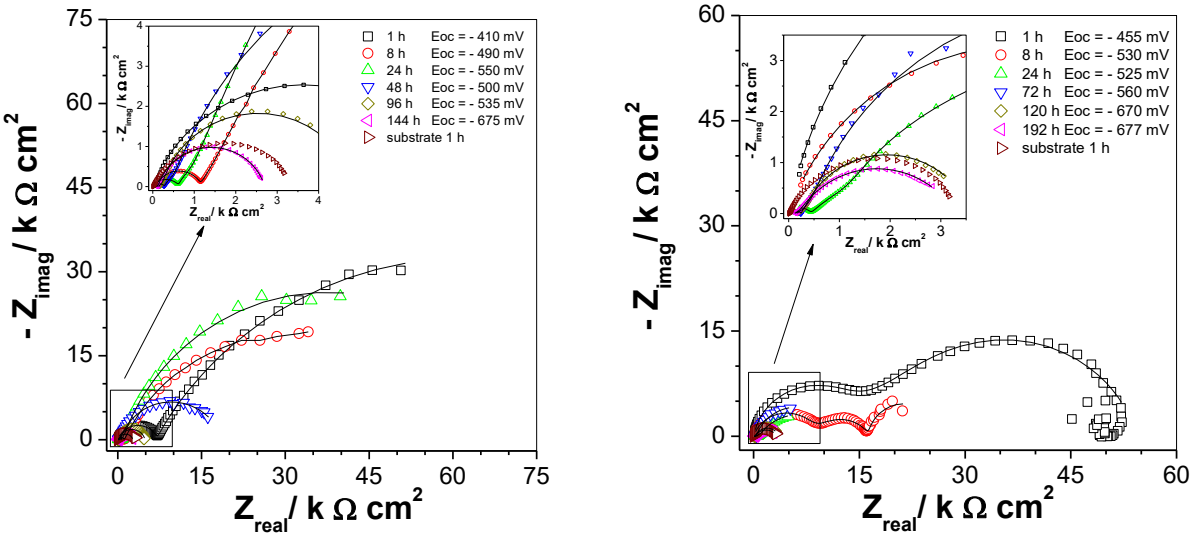

(A) (B)

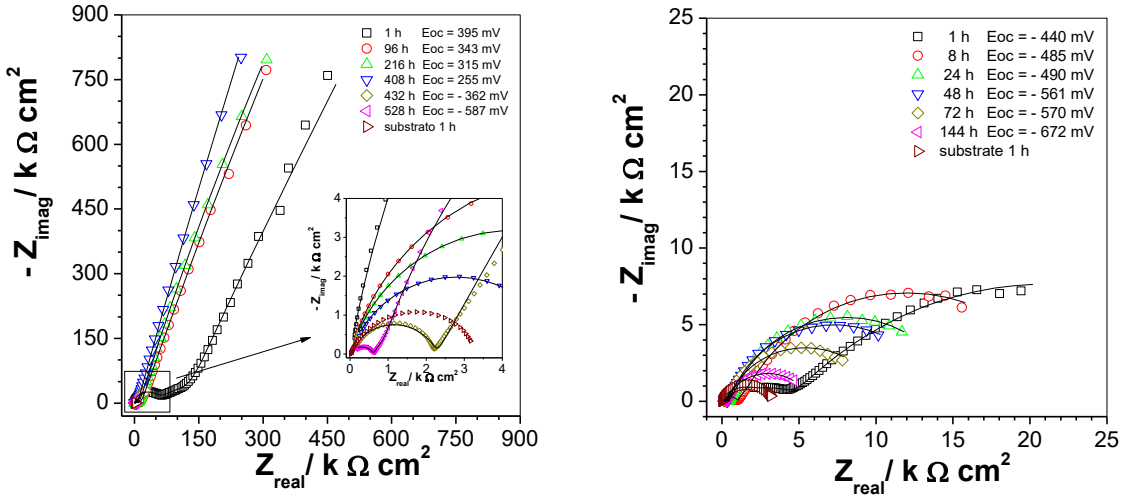

(C) (D)

Eclética Química Journal, vol. 44, n. 4, 2019, 27-56
ISSN: 1678-4618
DOI: 10.26850/1678-4618eqj.v44.4.2019.p27-56

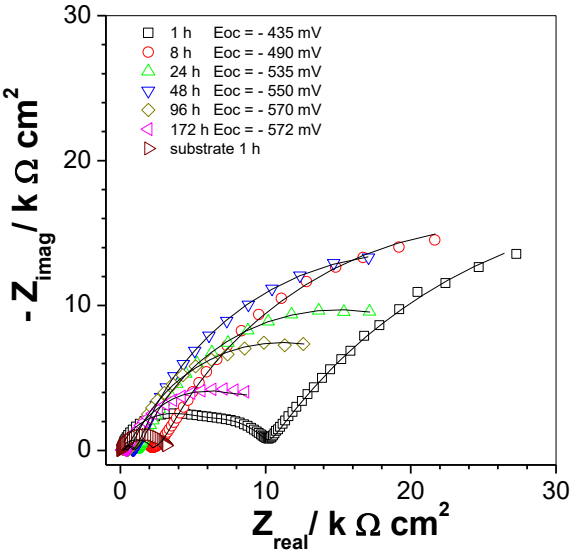

(E)

Figure 1S. Experimental (symbols) and fitted (solid line) complex plane plots for carbon steel coated with TEOS / MPTS doped with Ce(IV) ions: (A) 0 ppm, (B) 300 ppm, (C) 500 ppm, (D) 700 ppm and (E) 900 ppm with different immersion times in 0.1 mol L^{-1} NaCl.

Comparing the different diagrams, it can be verified that the coating doped with 500 ppm provides the highest impedance response, confirming the best protection of the substrate. For a given frequency, *f*=10 mHz, the highest Z_{real} value was obtained for this sample (about 450 kΩ cm^2) while for the other samples the maximum value was near 50 kΩ cm^2 (300 ppm). Even after 408 h immersion this coating showed a Z_{real} (*f*=10 mHz) around 200 kΩ cm^2, which is much higher than for the remainder of the samples at the beginning of their exposure period.

Eclética Química Journal, vol. 44, n. 4, 2019, 27-56
ISSN: 1678-4618
DOI: 10.26850/1678-4618eqj.v44.4.2019.p27-56

Figure 2S shows the maps of elements distribution for the hybrid coating with 0 and 500 ppm Ce^{4+} ions before immersion and EDS spectra after 240 h of immersion in 0.1 mol L^{-1} NaCl solution.

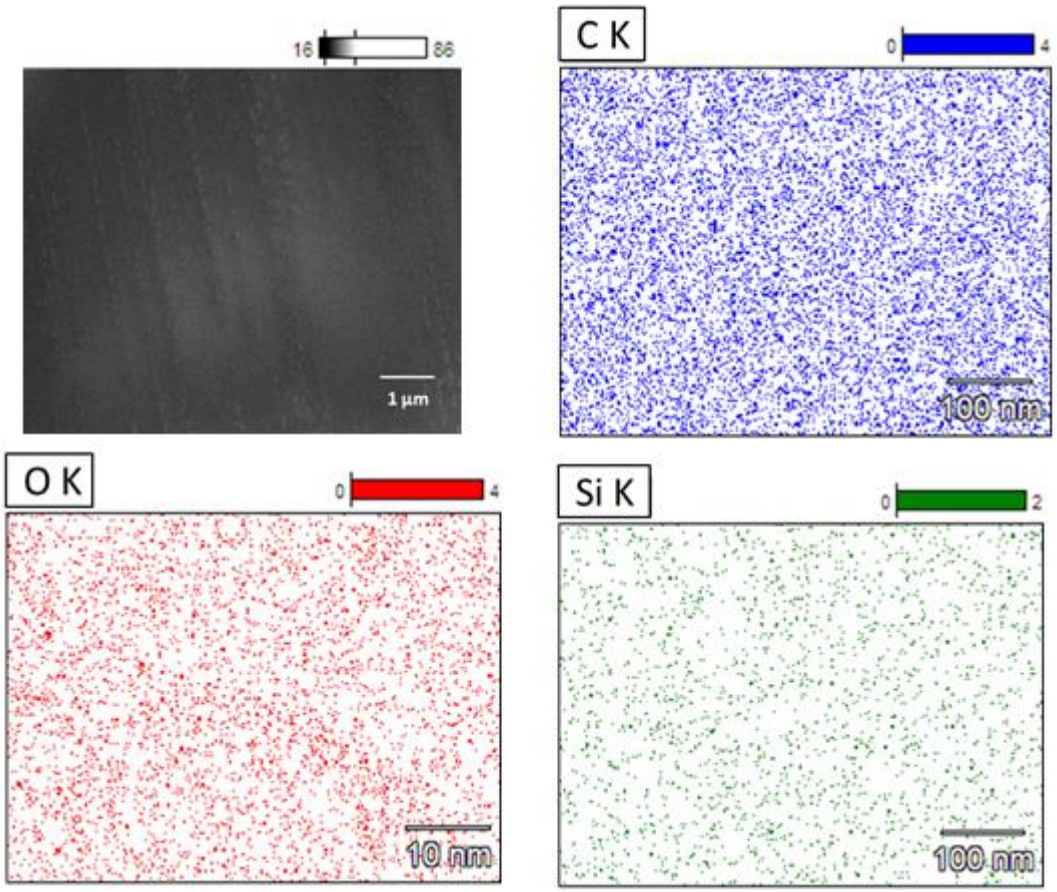

(A)

Eclética Química Journal, vol. 44, n. 4, 2019, 27-56
ISSN: 1678-4618
DOI: 10.26850/1678-4618eqj.v44.4.2019.p27-56

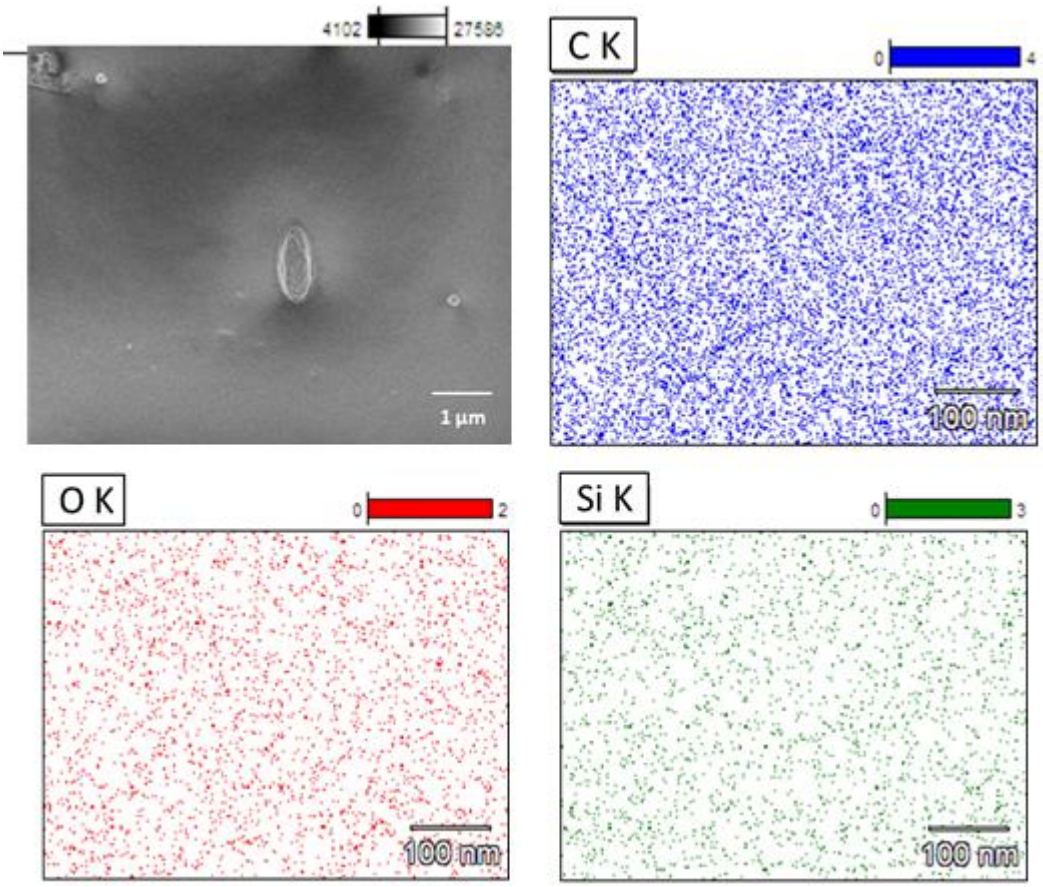

(B)

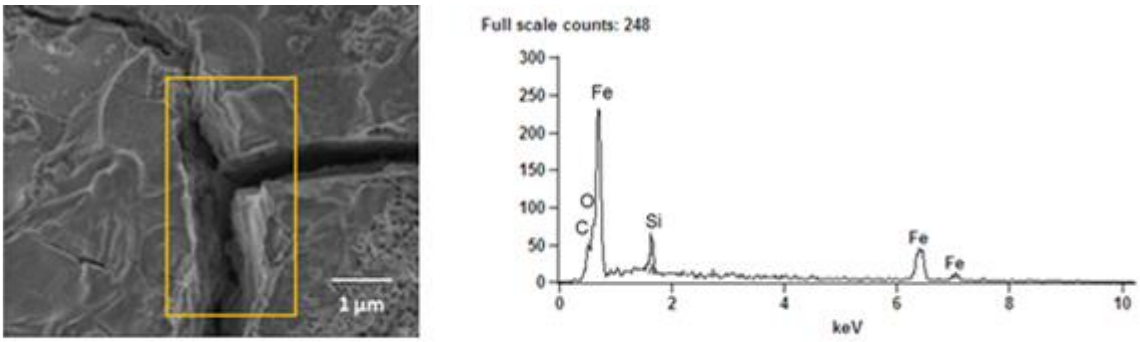

Quantitative Results for 0ppm Ce(IV) ions, EIS.

Element Line	*Weight %*
C K	14.57
O K	29.48
Si K	5.01
Fe L	50.94
Total	100.00

(C)

Eclética Química Journal, vol. 44, n. 4, 2019, 27-56
ISSN: 1678-4618
DOI: 10.26850/1678-4618eqj.v44.4.2019.p27-56

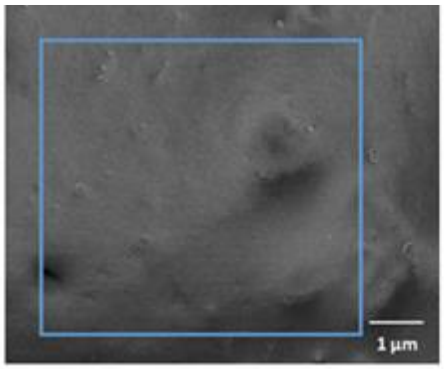

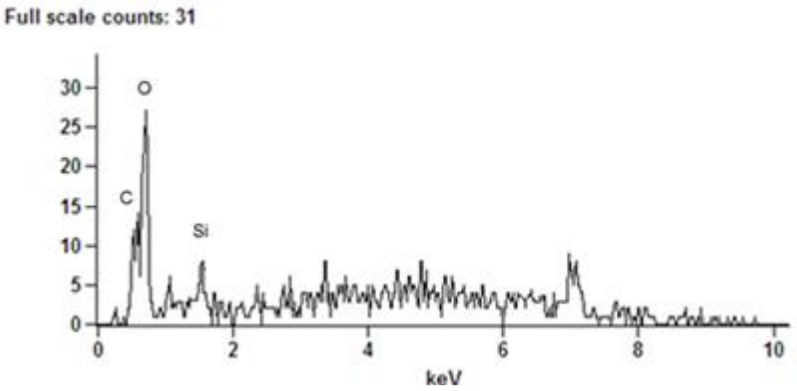

Quantitative results for 500 ppm Ce(IV) ions, EIS.

Element Line	*Weight %*
C K	32.25
O K	45.15
Si K	22.6
Total	100.00

(D)

Fig. 2S. Maps of elements distribution for the hybrid coating: (A) 0 ppm and (B) and 500 ppm Ce^{4+} ions before immersion and EDS spectra for samples with (C) 0 ppm and (D) 500 ppm Ce^{4+} ions after 240 h of immersion in 0.1 mol L^{-1} NaCl solution.

As mentioned in the main part of the manuscript different techniques were used trying to get information about the presence of cerium in the hybrid film and its main oxidation state. In this way, XPS, LIBS and UV-Vis analysis were performed. Due to the low concentration of cerium species in the hybrid films both XPS and LIBS techniques failed in detecting these ions in the hybrid film. However, insight on the presence and nature of cerium species in the doped film were obtained using UV-Vis technique.
Figure 3S shows the spectra obtained for aqueous solution resultant of extraction of cerium species from doped hybrid coatings prepared with different concentrations of Ce(IV) species.

Eclética Química Journal, vol. 44, n. 4, 2019, 27-56
ISSN: 1678-4618
DOI: 10.26850/1678-4618eqj.v44.4.2019.p27-56

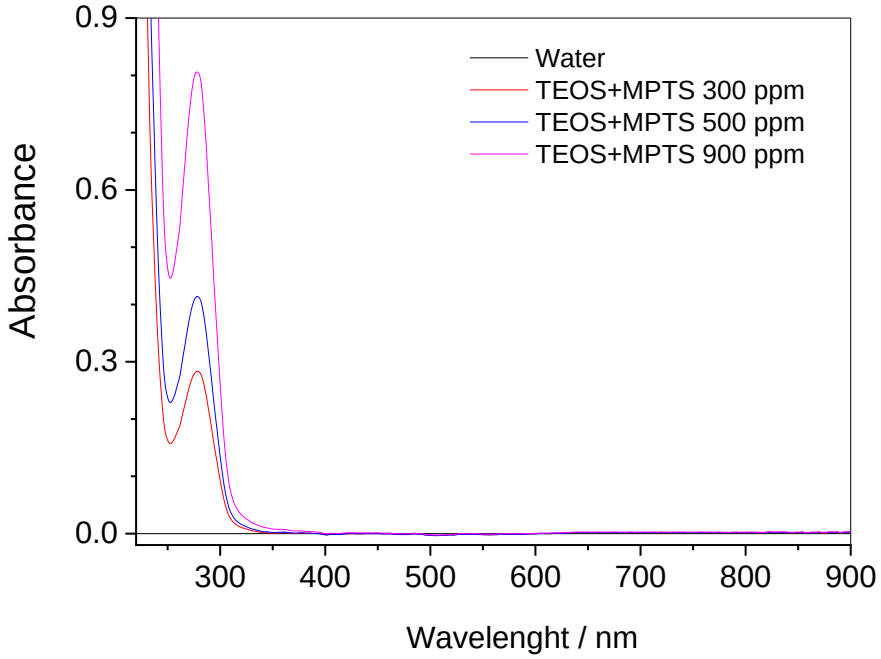

Figure 3S. Spectra obtained for aqueous solution resultant of extraction of cerium species from doped hybrid coatings prepared with different concentrations of Ce(IV) species.

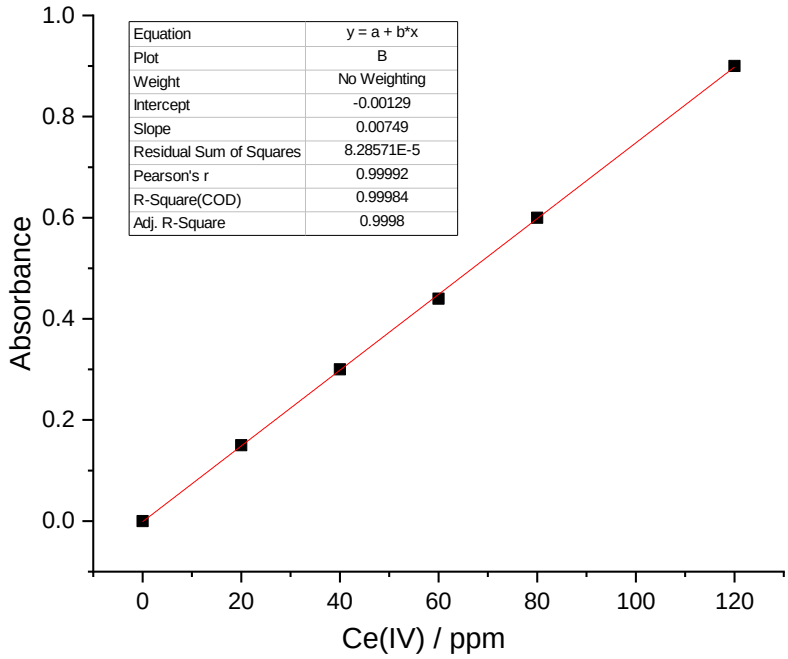

Figure 4S. Analytical curve for Ce(IV) ions ($Ce(SO_4)_2$) in aqueous solution at pH 6.5.

Eclética Química Journal, vol. 44, n. 4, 2019, 27-56
ISSN: 1678-4618
DOI: 10.26850/1678-4618eqj.v44.4.2019.p27-56

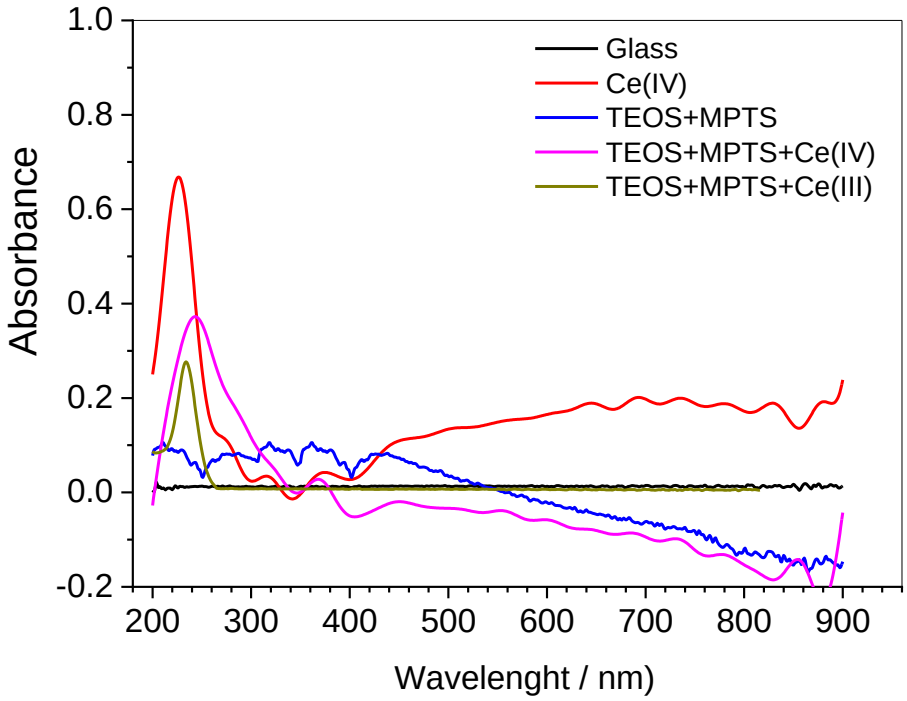

Figure 5S. Spectra obtained for cerium salt, glass and solid hybrid films with 0 ppm and 500 ppm of cerium deposited onto the glass.

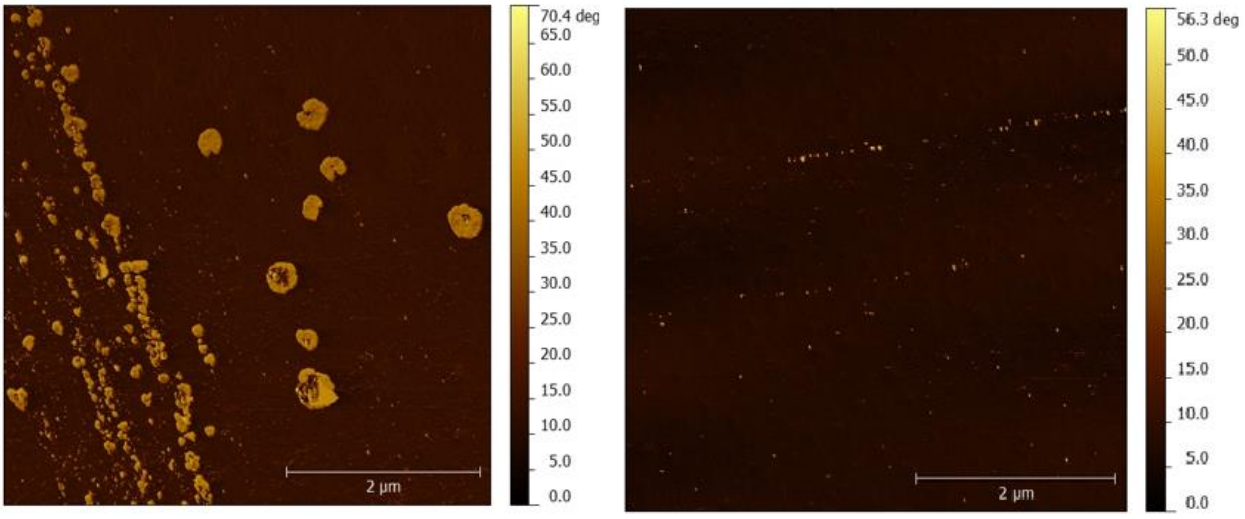

(A) (B)

Figure 6S. AFM images from TEOS / MPTS hybrid films prepared with: (**A**) 300 ppm Ce(III) and (**B**) 300 ppm of Ce(IV).

Eclética Química Journal, vol. 44, n. 4, 2019, 27-56
ISSN: 1678-4618
DOI: 10.26850/1678-4618eqj.v44.4.2019.p27-56

Table 1S. Results of the fitting procedure of the experimental EIS data with the EEC presented in Fig. 4 for a carbon steel sample coated with TEOS / MPTS and 0 ppm Ce(IV) in 0.1 mol L^{-1} NaCl solution.

Time / h	1	8	24	48	96	144
CPE_1-T / μFcm^{-2} $s^{\alpha-1}$	0.13 (2)*	0.4 (4)	1.3 (12)	4.4 (2.4)	3.2 (6)	1.5 (11)
α_1	0.78 (0.2)	0.70 (0.5)	0.6 (1.7)	0.5 (3.6)	0.5	0.5
R_1 / kΩ cm^2	7.0 (0.4)	1.1 (0.3)	0.66 (1.0)	0.30 (1.4)	0.16 (0.8)	0.10 (0.5)
CPE_3-T / μFcm^{-2} $s^{\alpha-1}$	57 (0.5)	84 (0.4)	107 (1.0)	154 (1.6)	174 (1.8)	277 (1.2)
α_2	0.7 (0.6)	0.7 (0.3)	0.73 (0.5)	0.72 (0.8)	0.7 (0.7)	0.8 (0.5)
R_3 / kΩ cm^2	103 (2.7)	59 (1.7)	107 (6.2)	27 (6.4)	5.1 (1.7)	2.7 (1.0)
$\chi 2$ / 10^{-3}	0.6	0.4	1.7	0.5	0.7	0.3

* The % errors associated with each estimative are given in parentheses.

Table 2S. Results of the fitting procedure of the experimental EIS data with the EEC Fig. 5 for carbon steel coated with TEOS / MPTS doped with 300 ppm of Ce(IV), in 0.1 mol L^{-1} NaCl.

Time / h	1	8	24	72	120	192
CPE_1-T / μFcm^{-2} $s^{\alpha-1}$	0.008 (2)*	0.03 (3.5)	0.86 (5.6)	1.1 (12)	1.8 (19)	2.0 (1.9)
α_1	0.9 (0.2)	0.80 (0.3)	0.58 (0.7)	0.56 (1.5)	0.53 (2.6)	0.5
R_1 / kΩ cm^2	16 (0.9)	8.2 (2)	0.44 (0.3)	0.24 (0.3)	0.17 (0.6)	0.13 (0.3)
CPE_2-T / μF cm^{-2} $s^{\alpha-1}$	0.05 (10)	1.3 (27)	508 (3)	649 (6)	288 (12)	184 (15)
α_2	1.0	0.7	0.50 (1.3)	0.73 (1.8)	0.68 (2.8)	0.65 (3)
R_2 / kΩ cm^2	4.6 (16)	1.8 (9.6)	3.2 (11)	0.93 (18)	0.21 (8.4)	0.14 (11)
CPE_3-T / μFcm^{-2} $s^{\alpha-1}$	0.72 (3)	5.5 (9.5)	302 (7.7)	368 (12)	509 (6.8)	342 (8.7)
α_3	0.7	0.7 (3.2)	0.92 (4.3)	0.89 (4.5)	0.82 (2)	0.65 (1.5)
R_3 / kΩ cm^2	34 (2.7)	6.6 (5.3)	13 (6.2)	11 (2.0)	3.2 (0.7)	3.0 (0.5)
$\chi 2$ / 10^{-3}	0.20	0.20	0.17	0.60	0.41	0.12

* The % errors associated with each estimative are given in parentheses.

Table 3S. Results of the fitting procedure of the experimental EIS data with the EEC Fig. 5 for carbon steel coated with TEOS / MPTS doped with 500 ppm of Ce(IV), in 0.1 mol L^{-1} NaCl.

Time / h	1	96	216	408	432	528	688
CPE_1-T / μFcm^{-2} $s^{\alpha-1}$	0.016 (3)*	0.04 (1.5)	0.05 (1.7)	0.07 (1.7)	0.1 (3.6)	0.45 (4.5)	2.0 (2.4)
α_1	0.88 (0.4)	0.81 (0.2)	0.81 (0.2)	0.79 (0.2)	0.7 (0.4)	0.67 (0.5)	0.5
R_1 / kΩ cm^2	60 (2)	8.5 (0.5)	8.5 (0.4)	5.5 (0.3)	2.1 (0.3)	0.62 (0.2)	0.11(0.2)
CPE_2-T / μFcm^{-2} $s^{\alpha-1}$	2 (15)	6.2 (16)	6.2 (16)	7.2 (14)	107 (9)	221 (6.8)	279 (15)
α_2	0.65 (6.4)	0.8 (3.6)	0.8 (3.6)	0.84 (2.9)	0.76 (3)	0.75 (1)	0.7 (2.8)
R_2 / kΩ cm^2	106 (11)	16 (29)	16 (29)	13 (28)	5.1 (23)	1.0 (16)	0.20 (25)
CPE_3-T / μFcm^{-2} $s^{\alpha-1}$	7.64 (5)	4.7 (23)	4.7 (23)	4.5 (23)	96 (12)	136 (12)	200 (21)
α_3	0.83 (3)	0.79 (3.5)	0.79 (3.5)	0.81 (3.1)	0.8 (3.8)	0.85 (3.2)	0.7 (3.9)
R_3 / kΩ cm^2	3510 (12)	27500 (11)	16000 (11)	47300 (27)	95 (3.2)	35 (1.8)	3.3 (1.3)
$\chi 2$ / 10^{-3}	1.69	0.13	0.13	0.11	0.39	0.26	0.18

* The % errors associated with each estimative are given in parentheses.

Eclética Química Journal, vol. 44, n. 4, 2019, 27-56
ISSN: 1678-4618
DOI: 10.26850/1678-4618eqj.v44.4.2019.p27-56

Table 4S. Results of the fitting procedure of the experimental EIS data with the EEC Fig. 5 for carbon steel coated with TEOS / MPTS doped with 700 ppm of Ce(IV), in 0.1 mol L^{-1} NaCl.

Time / h	1	8	24	48	72	144
CPE_1-T / μF cm^{-2} $s^{\alpha-1}$	0.15(5.4)*	0.47 (4.3)	1.0 (6.6)	4.9 (0.5)	5.0 (3)	2.2 (1.0)
α_1	0.74 (0.6)	0.68 (0.5)	0.62 (0.9)	0.5	0.5	0.5
R_1 / kΩ cm^2	2.5 (1.8)	1.0 (0.3)	0.46 (0.3)	0.35 (0.1)	0.28 (0.6)	0.15 (0.1)
CPE_2-T / μF cm^{-2} $s^{\alpha-1}$	3.7 (13)	170 (1.6)	203 (8.5)	242 (5.5)	237 (3.6)	355 (4.8)
α_2	0.68 (3.1)	0.7	0.78 (2.0)	0.78 (1.3)	0.7	0.7 (1)
R_2 / kΩ cm^2	1.8 (4.5)	5.1 (11)	1.3 (24)	1.0 (15)	0.49 (9.6)	0.39 (11)
CPE_3-T / μF cm^{-2} $s^{\alpha-1}$	149 (0.4)	65 (4)	105 (16)	128 (10)	153 (5.7)	176 (10)
α_3	0.50 (1.0)	0.9 (3)	0.84 (4.5)	0.86 (3)	0.89 (1.8)	0.78 (2.4)
R_3 / kΩ cm^2	43 (4)	17 (3.7)	14 (1.8)	12.8 (0.8)	10 (1.5)	5.2 (0.6)
$\chi 2$ / 10^{-3}	0.13	0.41	0.20	0.15	1.8	0.10

* The % errors associated with each estimative are given in parentheses.

Table 5S. Results of the fitting procedure of the experimental EIS data with the EEC Fig. 5 for carbon steel coated with TEOS / MPTS doped with 900 ppm of Ce(IV), in 0.1 mol L^{-1} NaCl.

Time / h	1	8	24	48	96	172
CPE_1-T / μF cm^{-2} $s^{\alpha-1}$	0.05 (3)*	0.18 (3)	0.25 (5)	0.32 (4.5)	1.4 (7.7)	2.7 (3)
α_1	0.81 (0.3)	0.73 (0.3)	0.72 (0.6)	0.70 (0.5)	0.58 (1.0)	0.5
R_1 / kΩ cm^2	6.4 (1.0)	2.2 (0.3)	1.0 (0.4)	0.8 (0.3)	0.50 (0.6)	0.19 (0.7)
CPE_2-T (μF cm^{-2} $s^{\alpha-1}$)	1.4 (8)	89 (4.2)	95 (23)	130 (17)	133 (17)	186 (16)
α_2	0.74 (2)	0.7	0.79 (5.4)	0.79 (4.2)	0.73 (4.2)	0.64 (3.6)
R_2 / kΩ cm^2	3.7 (2.4)	1.4 (7.7)	0.6 (20)	0.78 (20)	0.5 (15)	0.45 (16)
CPE_3-T / μF cm^{-2} $s^{\alpha-1}$	207 (0.7)	123 (2.7)	166 (13)	165 (14)	217 (11)	214 (14)
α_3	0.64 (0.8)	0.73 (1)	0.77 (2.4)	0.79 (2.8)	0.81 (2.7)	0.79 (3.8)
R_3 / kΩ cm^2	57 (3.2)	47 (2)	27 (1)	37 (1.0)	21 (2)	13 (4)
$\chi 2$ / 10^{-3}	0.10	0.36	0.24	0.19	0.41	1.2

* The % errors associated with each estimative are given in parentheses.

Eclética Química Journal, vol. 44, n. 4, 2019, 27-56
ISSN: 1678-4618
DOI: 10.26850/1678-4618eqj.v44.4.2019.p27-56